Inducible cell-specific mouse models for paired epigenetic and transcriptomic studies of microglia and astroglia

Authors: Ana J. Chucair-Elliott,[1 §] Sarah R. Ocañas,[1,2 §] David R. Stanford,[1] Victor A. Ansere,[1,2] Kyla B. Buettner,[1,2] Hunter Porter,[1,3] Nicole L. Eliason,[4] Justin Reid,[5] Amanda L. Sharpe,[4] Michael B. Stout, [6] Michael J. Beckstead,[5] Benjamin F. Miller, [5] Arlan Richardson,[7,8] Willard M. Freeman[1,8*]

[1]Genes & Human Disease Program, Oklahoma Medical Research Foundation, Oklahoma City, OK USA. [2]Department of Physiology, University of Oklahoma Health Sciences Center, Oklahoma City, OK USA, [3]Oklahoma Center for Neuroscience, University of Oklahoma Health Sciences Center, Oklahoma City, OK USA, [4]Department of Pharmaceutical Sciences, University of Oklahoma Health Sciences Center, Oklahoma City, OK USA, [5]Aging & Metabolism Program, Oklahoma Medical Research Foundation, Oklahoma City OK USA, [6]Department of Nutritional Sciences, University of Oklahoma Health Sciences Center, Oklahoma City, OK USA,[7]Department of Biochemistry, University of Oklahoma Health Sciences Center, Oklahoma City, OK, USA, [8]Oklahoma City Veterans Affairs Medical Center, Oklahoma City, OK USA

To whom correspondence should be addressed: [*]Willard M. Freeman, Genes & Human Disease Program, Oklahoma Medical Research Foundation, 825 NE 13th Street, Oklahoma City, OK 73104, USA.

Tel: 405-271-3139

Fax: 405-271-2536

E-mail address: bill-freeman@omrf.org

[§]*These authors contributed equally*

Abstract

Epigenetic regulation of gene expression occurs in a cell type-specific manner. Current cell-type specific neuroepigenetic studies rely on cell sorting methods that can alter cell phenotype and introduce potential confounds. Here we demonstrate and validate a Nuclear Tagging and Translating Ribosome Affinity Purification (NuTRAP) approach for temporally controlled labeling and isolation of ribosomes and nuclei, and thus RNA and DNA, from specific CNS cell types. Paired analysis of the transcriptome and DNA modifications in astrocytes and microglia demonstrates differential usage of DNA methylation and hydroxymethylation in CG and non-CG contexts that corresponds to cell type-specific gene expression. Application of this approach in LPS treated mice uncovers microglia-specific transcriptome and epigenome changes in inflammatory pathways that cannot be detected with tissue-level analysis. The NuTRAP model and the validation approaches presented can be applied to any CNS cell type for which a cell type-specific cre is available.

Introduction

Significant advances are being made in understanding the epigenome and its relationship with gene expression in the brain[1-3]. However, the lack of approaches for paired analysis of DNA and RNA profiles at the cell type-specific level within the same animal is a significant limitation for the field, given that epigenetic processes differ across CNS cell types at the level of chromatin organization and DNA modifications[1,4]. Obtaining enriched cell populations by flow sorting requires cell surface markers but these markers can change with experimental conditions and cell sorting causes molecular, morphological, and functional changes, such as cell activation, that could confound studies[3,5,6]. Single cell approaches[7] may overcome some of the challenges of cell sorting but the scale of such studies, partial genomic coverage, restriction to only certain types of endpoints, and continued potential for brain dissociation artifacts are limitations.

This has led to development of transgenic labeling approaches to isolate RNA or DNA from specific cell types. Ribosome labeling and RNA isolation methods, such as Translating Ribosome Affinity Purification (TRAP[8]), and ribosome tagging (RiboTag[9]), are gaining acceptance across neuroscience studies examining the transcriptome. Similar approaches have been developed to transgenically tag and allow isolation of nuclei and thus DNA (Isolation of Nuclei TAgged in Specific Cell Types, INTACT)[10]. However, using separate transgenic mouse strains for DNA and RNA endpoints is a complicated and resource intensive approach.

Here we describe an approach where Nuclear Tagging and Translating Ribosome Affinity Purification (NuTRAP)[11] is combined with well-established cell-specific inducible cre-recombinase expressing systems[12,13] to perform paired transcriptomic and epigenomic analyses of specific CNS cell types in a temporally controllable manner from a single mouse. Demonstration studies with astrocytes and microglial provide: 1) cell type-specific enrichment of RNA and DNA, 2) novel insights into differential usage of DNA modifications in microglia and astrocytes, and 3) examples of cell-type specific transcriptomic and epigenomic responses that are only revealed when specific cell types are examined. These studies also provide a validation approach NuTRAP mouse lines crossed to any available cre driver line relevant to neuroscience studies.

Results

Schematics of the NuTRAP construct, experimental design, and key protocols for the analyses in the current study are represented in **Supplemental Figure 1**. Of note, the Aldh1l1-cre/ERT2; NuTRAP and Cx3cr1-cre/ERT2; NuTRAP models will be abbreviated when necessary, as Aldh1l1-NuTRAP and Cx3cr1-NuTRAP, respectively. Testing of Tamoxifen (Tam) administration, for cre induction, effects on the epigenome and transcriptome in the CNS found no long-lasting, significant effects on DNA modifications or gene expression[14].

Flow cytometry and immunohistochemical validation of the Aldh1l1-cre/ERT2$^+$; NuTRAP$^+$ mouse brain.

The Aldh1l1-cre/ERT2$^+$ mouse line has been reported as highly efficient and specific for DNA recombination in astrocytes[12]. We first crossed this line with the NuTRAP reporter mouse[11] to couple epigenomic and gene expression studies in astrocytes in a parallel fashion. As an initial validation of the model, Aldh1l1-NuTRAP mice were systemically delivered Tam for 5 consecutive days and a week after induction, brains were dissected for flow cytometry (FC) and immunohistochemistry (IHC) analyses. Single-cell suspensions of brains immunostained with ACSA-2 antibody, a pan-astrocytic marker[15], revealed a distinct EGFP$^+$ cell population present in the Aldh1l1-NuTRAP brains but not in the cre negative counterparts, consistent with the reported 10-20% astroglial cellularity in the rodent brain[16,17], Almost the entirety of the EGFP$^+$ cell population co-expressed ACSA-2, supporting that cre-mediated recombination upon Tam induction specifically targeted astrocytes **(Figure 1A-B)**.

Sagittal brain sections immunostained with cell-specific markers showed EGFP and mCherry colocalization in cells expressing the astrocytic marker GFAP, but not in cells expressing microglial (Cd11b), or neuronal (NeuN) markers **(Figure 1C**, **Supplemental Figure 2)**. In the absence of Tam induction Aldh1l1-NuTRAP mice did not display EGFP or mCherry expression **(Supplemental Figure 2)**, consistent with temporally-controlled, Tam-dependent induction of cre-recombinase under the control of the Aldh1l1 promoter.

Astrocyte transcriptome enrichment in the Aldh1l1-NuTRAP mice by TRAP-RNAseq.

Enrichment of EGFP-tagged polysomes was performed with the TRAP protocol. The resulting positive and negative fractions, as well as input fraction, were collected for RNA isolation. qPCR measurements showed significant enrichment of marker genes for astrocytes (Aldh1l1 and GFAP) in the positive fraction compared to input and negative fractions. Depletion of marker genes for

microglia (Cx3cr1, C1q, Itgam), neurons (Eno2, Npas4), and oligodendrocytes (Mog) was observed in the positive TRAP fraction compared to the other fractions **(Figure 2A)**. RNAseq analysis, as visualized by Principal Component Analysis (PCA), revealed separation of positive fraction from input, negative, and whole tissue samples in the first component **(Figure 2B)**. Cell type-specific marker gene lists were generated from prior cell sorting studies[18] **(Supplemental Table 4).** The distribution of cell type-specific gene expression showed enrichment of astrocytic genes and depletion of microglial, neuronal, and oligodendrocytic genes in the positive fraction relative to input **(Figure 2C-2D)**.

One prior study applied the RiboTag approach with the same Aldh1l1- cre/ERT2 line of mice[12]. In another recent study[19] the RiboTag approach with a Gfap-cre was used to target the astrocyte transcriptome. We compared the lists of astrocyte marker genes (BHMTC $p<0.05$, FC enrichment >5) generated in these studies with the data from the NuTRAP line developed here and found 127 ribosomal-tagging marker genes for astrocytes that are independent of ribosomal tagging approach or cre line **(Figure 2E, Supplemental Table 4)**. When this list of 127 ribosomal-tagging astrocyte marker genes was compared to previously-identified astrocyte markers from cell sorting studes[18], we found 12 isolation method independent astrocyte marker genes **(Figure 2F, Supplemental Table 4)**. Taken together, these comparisons demonstrate a commonality to astrocyte enriched genes with some minor differences in RiboTag versus NuTRAP and Aldh1l1 versus Gfap cre lines. Astrocyte enriched transcripts further demonstrated over-representation of genes critical in astrocyte physiological functions[12,19,20] such as cholesterol synthesis and transport, fatty acid metabolism, receptors/channels, complement/immune mediators and synapse modification (formation, function, and elimination) **(Supplemental Figure 3)**. These findings are collectively in agreement with the normal physiology of astrocytes in the brain and demonstrate specific targeting and enrichment of astrocyte transcripts in the Aldh1l1-NuTRAP model.

Validation of astrocytic epigenome enrichment in the Aldh1l1-NuTRAP mouse brain by INTACT-BSAS.

Nuclear preparations of Aldh1l1-NuTRAP were subjected to INTACT isolation with streptavidin magnetic beads for separation of negative and positive (biotinylated) nuclei. To assess purity of putatively astrocytic nuclei in the positive fraction, nuclei were evaluated for expression of mCherry by confocal microscopy imaging **(Figure 3A-B)**. Biotinylated, mCherry$^+$ nuclei covered by streptavidin beads (that fluoresce in the red channel[10]) were evident in the positive fraction **(Figure 3A)** and comprised 90% of the positive fraction **(Figure 3B)**. With the predicate that mCG

in gene promoters is inversely related to transcriptional activation, Bisulfite Amplicon Sequencing (BSAS) analysis was performed to measure the percentage genomic CG methylation (mCG) in the promoter region of selected astrocytic (Fabp7), microglial (Gpr84), and neuronal (Eno2) marker genes **(Figure 3C)**. In the positive fraction, hypomethylation of the Fabp7 gene promoter as compared to input and negative fractions correlated with increased gene expression found by RNAseq **(Figure 3D**), supporting the astrocytic identity of the INTACT-isolated nuclei and DNA in the positive fraction. A minor trend to mCG hypermethylation of the non-astrocytic gene promoters Gpr84 and Eno2 coincided with depletion of microglial and neuronal gene expression in the positive fraction.

Flow cytometry and immunohistochemical validation of the Cx3cr1-cre/ERT2^{+}; NuTRAP^{+} mouse brain.

Validation of the Cx3cr1-NuTRAP line was performed with a similar approach as above. Tam was administered for 5 consecutive days and in order to avoid labeling of circulating monocytes in the tissue, which unlike resident microglia are short-lived and rapidly renew themselves[21], brain tissue collection was delayed until 3-4 weeks after treatment. Single cell suspensions of brain tissue immunostained with antibody against CD11b, a microglia marker, revealed a distinct EGFP^{+} cell population present in the Cx3cr1-NuTRAP brains but not in the cre negative subjects, consistent with the reported 5-10% microglial constituency of the mouse brain[22]. The EGFP^{+} cell population almost completely co-expressed CD11b, evidence of cell-specific cre recombination for the microglial lineage **(Figure 4A-B, Supplemental Figure 4)**. The evidence for microglia-specific recombination was next tested with IHC. Sagittal brain sections immunostained with cell-specific markers showed EGFP and mCherry colocalization in cells expressing CD11b **(Figure 4C**, **Supplemental Figure 4)**. In the absence of Tam induction, FC immunolabelings indicated that Cx3cr1-NuTRAP mice displayed a small EGFP^{+} cell population that mostly expressed CD11b. Such observation was in agreement with reported findings using the same cre line[5], and was not clearly detected with the sensitivity of IHC **(Supplemental Figure 5)**.

RNAseq validation of microglial transcriptome enrichment in the Cx3cr1-NuTRAP mouse brain by TRAP-RNAseq.

TRAP isolation was performed as described above. Initial qPCR validation of the TRAP-isolated RNA from all three fractions showed significant enrichment of marker genes for microglia (Cx3cr1, C1q, and Itgam) in the positive fraction compared to input and negative fractions. Significant depletion of marker genes for astrocytes (GFAP and Aldh1l1) and oligodendrocytes (Mog), as

well as a trend in neurons (Eno2 and Npas4), was observed in the positive TRAP fraction compared to the other fractions **(Figure 5A)**. RNAseq was performed on input, negative, and positive fractions from TRAP isolation, as well as whole tissue. Transcriptome profiles revealed separation of positive fraction from all other groups **(Figure 5B)** by PCA. Fold change enrichment in the positive TRAP fraction versus the input was compared to microglial marker genes lists from cell sorting studies. Enrichment of microglial genes and depletion of astrocytic, neuronal, and oligodendrocytic genes was observed in the positive fraction relative to input **(Figure 5C-5D)**. The same Cx3cr1-cre/ERT2(Jung) line as used here has been used with RiboTag enrichment of microglial RNA[5]. In another study, the Cx3cr1-creErt2/+(Litt) line was crossed with a TRAP mouse model[3]. We compared the lists of microglial marker genes with FC>5 ($p<0.05$, positive fraction/input) in these studies[3,5] with the Cx3cr1-NuTRAP (Present study). We identified 142 ribosomal-tagging common microglial marker genes **(Figure 5E, Supplemental Table 5)**. Comparing the ribosomal-tagging microglial marker genes with previously established microglial marker genes from cell sorting studies[18] revealed 101 isolation method-independent microglial marker genes **(Supplemental Table 5)**.

Genes enriched in the microglia transcriptome included an overrepresentation of genes regulated by PU.1 (also known as Spi1), a transcription factor that shapes the homeostatic functions of microglia[23] **(Supplemental Figure 5)**. Collectively, data provide ample support that the Cx3cr1-NuTRAP model is suitable for studying the microglia transcriptomic signatures of the brain in both homeostatic and stress settings.

Transcriptome comparison between Aldh1l1-NuTRAP and Cx3cr1-NuTRAP positive fractions by regulator and pathway analyses confirmed cell-specific enrichments in agreement with brain astrocytes and microglia, respectively **(Supplemental Figure 6)**.

Validation of microglial epigenome enrichment in the Cx3cr1-NuTRAP mouse brain by INTACT-BSAS.

In parallel with the TRAP protocol described above, nuclear preparations of Cx3cr1-NuTRAP were subjected to INTACT isolation with streptavidin magnetic beads for separation of negative and positive (biotinylated) nuclei. To assess purity of putatively microglial nuclei in the positive fraction, nuclei were evaluated for expression of mCherry by confocal microscopy imaging. Biotinylated, mCherry+ nuclei were covered by streptavidin beads **(Figure 6A)** and reached over 90% purity in the positive fraction **(Figure 6B)**. CG methylation around the promoter region of selected astrocytic (Fabp7), microglial (Gpr84), and neuronal (Eno2) genes **(Figure 6C)**

demonstrated hypomethylation of the Gpr84 gene promoter correlated with increased gene expression levels assessed by RNAseq in the positive fraction **(Figure 6D)**, as compared to input and negative fractions was indicative of the microglial identity of the nuclei isolated in the positive fraction by INTACT. In addition, we observed no significant change in the cytosine methylation of Fabp7 and Eno2 gene promoters associated with depletion of astrocytic and neuronal gene expression in the positive fraction.

Cell-specific epigenetic findings by Whole Genome Oxidative Bisulfite Sequencing comparing Aldh1l1-NuTRAP and Cx3cr1-NuTRAP models.

The landscape of the brain epigenome at a single-base resolution, and at the cell type-specific level, remains largely unknown[2,24]. Moreover, no studies have compared the methylome of different cell types, such as astrocytes and microglia, using a combination of inducible cre-recombinase and NuTRAP technologies. Upon validation of the cell-specific identity of the INTACT-isolated gDNA from positive fractions by BSAS **(Figure 3** and **Figure 6)**, WGoxBS sequencing libraries were constructed from the DNA samples isolated from input, negative, and positive INTACT fractions. Genome-wide levels of mCG, hmCG, mCH, and hmCH (see **Supplemental Figure 7** for conversion efficiency controls) were compared across fractions and cell types. The analysis revealed that global mCG levels are similar (~70%) between the Aldh1l1-NuTRAP and Cx3cr1-NuTRAP positive fractions **(Figure 7A)**. Of interest, levels of hmCG were lower in the Cx3cr1-NuTRAP positive fraction and mCH levels were lower in both positive fractions as compared to input and negative fractions **(Figure 7B-C)**. These data demonstrate that microglia use less cytosine hydroxymethylation compared to other cell types including astrocytes **(Figure 7B)**. The analysis of mCH levels showed a significantly lower level of mCH in the Aldh1l1l-NuTRAP and Cx3cr1-NuTRAP positive fractions with respect to their negative fractions. The lower level of non-CG methylation was more pronounced in microglia, being significantly less than the input. This is consistent with the concept that mCH is concentrated in neurons[1] and provides more specific detail that this is true when astrocytes or microglial alone are examined. As previously reported for the brain[14,25,26], no non-CG hydroxymethylation (hmCH) was detected in any of the samples analyzed **(Figure 7D)**. To uncover potential cell type-specific differences in mCG patterns, methylation across cell-type marker genes (from -4kb in respect to the TSS and +4b from the TES) was compared for astrocytes **(Figure 7E)** and microglia **(Figure 7H)**. In Aldh1l1-NuTRAP INTACT positive fractions, but not Cx3cr1-NuTRAP INTACT positive fractions, hypomethylation upstream, within, and downstream the gene body **(Figure 7F)** was evident across astrocyte marker genes as compared to input and Cx3cr1-NuTRAP positive fractions. This

correlates with the higher levels of mRNA expression of these genes in Aldh1l1-NuTRAP TRAP positive fraction **(Figure 7G)**. Similarly, only in the Cx3cr1-NuTRAP INTACT positive fraction, hypomethylation upstream, within, and downstream the gene body of microglial markers genes was evident **(Figure 7I)** and in agreement with higher mRNA expression of these genes in microglia **(Figure 7J)**.

CG dinucleotides are found far less frequently than other dinucleotide pairs (<1% dinucleotide pairs) and are clustered together in CpG islands. Definitions for the regions around the CpG islands have been established and include shores (2Kb upstream and downstream from CpG island) and shelves (2Kb upstream and downstream from shores). Despite their high CG content, CpG islands are mainly unmethylated while methylation is higher in shores and shelves[27]. Analysis of methylation and hydroxymethylation levels covering CpG islands, shores, and shelves revealed that the shores and shelves of Cx3cr1-NuTRAP INTACT positive fractions cells had significantly higher mCG levels **(Supplemental Figure 8 A-B)** and significantly lower hmCG levels **(Supplemental Figure 8 C-D)** compared to the other groups. The findings allow us to speculate that while low levels of mCG and hmCG are conserved in CpG islands across the genome, epigenetic signatures found in shores and shelves might differentiate microglia from the other cell types of the brain.

More than two-thirds of the mammalian genome consists of repetitive elements[28], including long terminal repeats (LTR), long interspersed nuclear elements (LINE), short interspersed nuclear elements (SINE), major satellites, and simple repeats[29]. The biological significance of repetitive element methylation/hydroxymethylation is unknown and has been difficult to explore in a cell type-specific manner. Input and positive fractions from Aldh1l1-NuTRAP and Cx3cr1-NuTRAP brain samples were analyzed for mCG, hmCG, and mCH content in whole genome, repeats, and non-repeats (**Supplemental Figure 9 A-C)**. In general, there were either no or minimal differences in mCG levels evident in repeat elements **(Supplemental Figure 9D)**. However, hmCG and mCH repeat element (SINE, LINE, LTR, and simple repeat) levels were lower in the Cx3cr1-NuTRAP INTACT positive fraction as compared to the other groups. These findings identify epigenetic markers that are microglia- and repetitive element-specific.

RNAseq analysis of microglial transcriptome 24 hours after LPS challenge in the Cx3cr1-NuTRAP mouse brain.

To probe the utility of using NuTRAP models to identify cell type-specific molecular changes not observable in tissue level analyses, we performed an acute LPS administration paradigm in the

Cx3cr1-NuTRAP model. Systemic delivery of LPS is commonly used to study microglial responses in the brain[30-32]. Toll-like receptors (TLRs) are pattern recognition receptors expressed by innate immune cells, such as microglia, and recognize and respond to conserved structural motifs called pathogen-associated molecular patterns (PAMPs) including LPS, initiating a cascade of molecular reactions resulting in the upregulation of pro-inflammatory cytokines and chemokines[33].

To interrogate the microglial transcriptome and epigenome Cx3cr1-NuTRAP mice were administered a single i.p. injection of 5 mg/kg LPS or PBS as sham control. To confirm induction of inflammation by LPS, plasma and brain tissues were analyzed for content of inflammatory cytokines. Circulating IL6, TNF, and IFNɣ contents were elevated as early as at 4 hours post LPS treatment and specifically IL-6 remained elevated in plasma and brain after 24 hours **(Supplemental Figure 10 A-B)**. Brain sections were also immunostained with mCherry and CD11b antibodies to visualize the specificity of cre-mediated recombination in microglial cells in both treatment groups **(Supplemental Figure 10C)**. At 24 hours post LPS or PBS injection, brains from Tam-induced Cx3cr1-NuTRAP mice were collected for TRAP and INTACT protocols. Initially, TRAP-isolated RNA samples were processed for qPCR analysis of genes associated with microglia and downstream activation of the TLR4 pathway in input, negative, and positive fractions **(Supplemental Figure 11)**. Microglial markers were highly enriched in the positive fraction of PBS- and LPS-treated mice compared to all input and negative fractions. Additionally, induction of C1qa, Itgam, Myd88, Il1α, Il1β, and Tnfα were evident in LPS TRAP samples but were not observable in input or negative fractions **(Supplemental Figure 11)**. In the design of the RNAseq experiment, libraries were made from RNA from input and positive TRAP fractions, excluding the negative fraction for further analyses. PCA revealed separation of samples by fractionation in the first component (68.96 %), and separation of samples by treatment in the second component (13.03%) **(Figure 8A)**. Differential gene expression in response to LPS was compared between positive fraction and input. LPS-induced changes demonstrate higher fold changes when microglial RNA is isolated by TRAP **(Figure 8B)** as also evident in heatmap presentation with hierarchical clustering of gene expression that differentiated input and positive fractions first and secondly by treatment **(Figure 8C)**. Collectively, the data suggest that the NuTRAP approach produced excellent microglia-specific gene enrichment, microglial responses to a stimulus, such as LPS, can be revealed, or are more pronounced when compared to analysis of whole tissue.

Although a handful of studies have suggested DNA methylation as a principal regulator of microglial activation[34], little microglia-specific *in vivo* evidence is available to compare DNA methylation with concurrent changes in transcriptomic response. By coupling LPS administration with the cell type-specific Cx3cr1-NuTRAP model we are able to interrogate dynamic changes in DNA methylation in $Cx3cr1^{+}$ (microglia) cells with their paired transcriptomic changes indicative of a pro-inflammatory response. Cx3cr1-NuTRAP mice were systemically administered 5 mg/kg LPS or PBS by ip injection and 24 hours after treatment and in parallel with the TRAP procedure, half brains were dissected for INTACT protocol and downstream applications. BSAS analysis of selected microglial (Gpr84, Aif1), astrocytic (Fabp7), and neuronal (Eno2) marker genes was conducted on input and INTACT-isolated positive fractions. The INTACT-isolated positive fraction exhibited lower CG methylation (mCG) in the promoter region of microglial marker genes Gpr84 and Aif1 as compared to input, regardless of treatment **(Supplemental Figure 12 A, C)**. Hypomethylation of the Gpr84 and Aif1 promoters in the positive fraction correlated with their respective increased gene expression by TRAP-RNAseq **(Supplemental Figure 12 B, D)**. There was no correlation between gene expression and methylation for the astrocytic marker Fabp7 or the neuronal marker Eno2 **(Supplemental Figure 12 E-H)**.

As the resident macrophages of the CNS, microglia are equipped with a number of TLRs, including TLR2 and TLR4. TLRs 2 and 4 recognize LPS as a PAMP and initiate an inflammatory cascade that acts through downstream mediators, like Myd88 and Ly96. To assess the effects of LPS administration on DNA methylation, BSAS of inflammatory genes (Tlr2, Myd88, Ly96) was conducted on INTACT-isolated DNA in parallel with TRAP-RNAseq. Upon LPS administration, the Tlr2 promoter was hypomethylated in the positive fraction but not input, when compared to their respective vehicle controls **(Figure 8D)**. Hypomethylation of the Tlr2 promoter in the positive fraction with LPS correlated with increased gene expression in the positive fraction with LPS **(Figure 8D)**. Myd88, a downstream effector of TLRs, showed decreased CG methylation in the positive fraction with LPS treatment when compared to PBS control, while the input had no change in Myd88 methylation with LPS treatment **(Figure 8E)**. The change in promoter mCG in the positive fraction with LPS was correlated to an increase in Myd88 gene expression **(Figure 8E)**. While the positive fraction showed a decrease in Ly96 methylation with LPS administration **(Figure 8F)**, there was no change in Ly96 gene expression **(Figure 8F)**. Of note, in the cases of Tlr2, Myd88, and Ly96 promoter methylation, the changes in methylation observed in the positive fraction were not apparent in the input. This highlights the importance of studying DNA modifications in a cell type-specific manner and the value of the Cx3cr1-NuTRAP model to study the relationship between microglia genomic methylation and transcriptome.

Lastly, to further demonstrate the utility of the NuTRAP system for additional molecular analyses, we examined microglial proliferation by stable isotopic labeling. This approach uses deuterium oxide (D_2O) in drinking water, which quickly equilibrates its labeling with the deoxyribose moiety[35]. The labeled deoxyribose moiety is then incorporated into DNA through de novo synthesis only, with no contribution of salvage pathways or repair processes. After 30 days of D_2O administration to Cx3cr1-NuTRAP mice INTACT isolation was performed and the DNA extracted. Incorporation of deuterium was determined through GC-MS in the positive fraction and input and found to be significantly greater in the positive fraction **(Supplemental Figure 13)** indicating that microglial replication is greater than the average of all CNS cellular populations[36].

In summary, the results offer extensive evidence to support the combination of inducible cre/lox and NuTRAP models as a suitable and powerful approach for the parallel study of the cell-specific epigenetic and transcriptomic signatures in the brain.

Discussion

Two of the main challenges that obstruct the interpretation of neuroepigenetic studies are the isolation of specific cell types from the complex milieu of the CNS and the lack of approaches to analyze both the transcriptome and epigenome of such cells. Combining TRAP and INTACT tagging into one construct that can be temporally controlled provides a tractable approach for cell type-specific paired analysis of the epigenome and transcriptome. We present the development, validation and application of this approach for astrocytes and microglia. These approaches could be applied to any CNS cell type for which there is an appropriate cre driver line. The inducible nature of the Cre-*Lox* systems used (Aldh1l1-cre/ERT2[12] and Cx3cr1-cre/ERT2[13]), in combination with the recently developed NuTRAP construct[11], also allows for temporal control of labeling of cell-specific nuclei and polyribosomes, avoiding the deleterious effects of constitutive DNA recombination during development and potential confounds from having developmental expression of the cre when studying adult/aged stages of the lifespan. To the best of our knowledge, this is the first study applying the NuTRAP model to neuroscience research, or using Tam-dependent induction. Importantly, these results also provide approaches for generation and validation of NuTRAP neuroscience models crossed to any relevant cell type-specific cre line.

The NuTRAP system combining TRAP and INTACT tagging approaches into one floxed construct was first described and applied to adipocytes[11]. The potential use in neuroscience research is relatively obvious as a number of reports describe the limitations of using cell sorting through surface markers. Importantly for glial research the very act of flow cytometry may change the activational state of these cells[5]. TRAP and INTACT isolations allow nucleic acids to be rapidly isolated from subcellular fractions decreasing the likelihood of isolation artifacts.

Validation of inducible cell type-specific NuTRAP models requires multiple steps to confirm the specificity of both the NuTRAP induction and the TRAP and INTACT isolations. The flow cytometry and imaging validation experiments demonstrated Tam-dependent cell type-specific induction of the NuTRAP construct in astrocytes and microglia. Transcriptomic studies demonstrated TRAP isolation of highly enriched astroglial RNA in the Aldh1l1-NuTRAP and microglial RNA in the Cx3cr1-NuTRAP positive fractions isolated by TRAP procedures. Validation of cell type-specific DNA poses a more challenging question but cell-type specific DNA modification patterns are consistent with the concept of cell type-specific hypomethylation of cell marker genes. Together these studies provide high confidence that these are valid models to be applied in a broad spectrum of neuroscience research studies ranging from brain aging, to neurodegenerative and neuropsychiatric studies. Moreover, the validation approach can be

applied to any new NuTRAP model and the protocols described here can be scaled-down to microdissected CNS tissue, such as a single hippocampus or retina sample (not shown).

These findings also reveal new insights into astrocyte and microglia biology. Non-neuronal cells have been reported to have less CG hydroxymethylation than other cells in the brain and also have lower non-CpG methylation[1]. While it is sometimes simplistically believed hydroxymethylation and non-CpG methylation are restricted to neurons these findings provide evidence that while CG hydroxymethylation and non-CG methylation levels may be lower in non-neuronal cell populations yet they are not absent. To date, there is no explanation for why hydroxymethylation is not evident in the non-CG context but as previously reported this modification is absent or at a level below detection[14,25].

To determine the sensitivity of cre/ERT2-NuTRAP approaches for the detection of molecular changes at the cell type-specific level that are not evident in tissue homogenates we acutely administered LPS to Cx3cr1-NuTRAP mice. Microglia-specific transcriptome and epigenome changes were revealed that could not be detected without affinity purification. Further, we demonstrated how our approach in combination with other labeling approaches, in this case D_2O, could help provide insight into how cell-specific genomic changes influence dynamic processes of the cell, such as replication. Collectively, our experiments demonstrated that the NuTRAP approach can be applied to CNS cell populations and INTACT approaches can be used to study DNA modifications, not only at the whole genome and gene promoter levels, but also in repeat elements of the genome, as shown here for the first time.

In light of the increasing interest in cell-specific contributions to the CNS epigenome[2,24] and transcriptome[3,5,12,19,20,30,31,37] landscapes, the use of transgenic inducible cre mouse models that allow for manipulation of specific floxed genes, or tagging of cell-specific nuclei/and or polysomes represent valuable research tools. Models using constructs such as INTACT[2], TRAP[8], and RiboTag[9], constitute critical advancements for DNA or RNA studies of specific cell types. However, the introduction of inducible-cre mouse lines in combination with NuTRAP technology, as validated in this study, is a powerful strategy in the interrogation of the cell type-specific dependent differences in the transcriptomes and epigenomes in the adult CNS.

Acknowledgements

The authors acknowledge the Laboratory for Molecular Biology and Cytometry Research at OUHSC for the use of the Core Facility, which provided flow cytometry services, the Cellular Imaging Core, at the Dean McGee Institute, OUHSC, for providing access to vibratome and confocal imaging equipment, and the Oklahoma Medical Research Foundation Clinical Genomics Center, which provided sequencing services. Computing for this project was performed at the OU Supercomputing Center for Education & Research (OSCER) at the University of Oklahoma (OU). The authors also acknowledge Adeline Machalinski (mouse colony management and genotyping), Robyn Berent (administrative support and lab management), P. Marlow for figure preparation, and Dr. Michael H. Elliott for critical scientific discussions during the preparation of this manuscript.

This work was supported by grants from the National Institutes of Health (NIH) P30AG050911, R56AG059430, R01AG059430, P20GM125528, T32AG052363, F31AG064861, P30EY021725, R01AG052606, Oklahoma Center for Adult Stem Cell Research (OCASCR), a program of the Oklahoma Tobacco Settlement Endowment Trust, and Presbyterian Health Foundation. This work was also supported in part by the MERIT award I01BX003906 from the United States (U.S.) Department of Veterans Affairs, Biomedical Laboratory Research and Development Service.

Methods

Animals

All animal procedures were approved by the Institutional Animal Care and Use Committee at the University of Oklahoma Health Sciences Center (OUHSC). Mice were purchased from the Jackson Laboratory (Bar Harbor, ME), bred, and housed in the animal facility at the OUHSC, under SPF conditions in a HEPA barrier environment. In separate breeding strategies Aldh1l1-Cre/ERT2$^{+/wt}$ males (stock number # 29655)[12] and Cx3cr1-Cre/ERT2$^{+/+}$ males (stock # 20940)[13] were mated with NuTRAP$^{flox/flox}$ females (stock # 029899)[11] to generate the desired progeny, Aldh1l1-cre/ERT2$^{+/wt}$; NuTRAP$^{flox/wt}$ (Aldh1l1-cre/ERT2^{+}; NuTRAP^{+}) and Cx3cr1-cre/ERT2$^{+/wt}$; NuTRAP$^{flox/wt}$ (Cx3cr1-cre/ERT2^{+}; NuTRAP^{+}). The cross of the Vav-iCre mouse model (stock # 008610)[38] with the NuTRAP$^{flox/flox}$ line did not show the specific labeling of brain microglia in agreement with a previous report[3], and was not used for further validations. DNA was extracted from mouse ear punch samples for genotyping. Mice (males and females) were ~3 months old at the time of performing experiments. Euthanasia prior to tissue harvesting was carried out either by cervical dislocation, or by cardiac perfusion with phosphate buffered saline (PBS), upon deeply anesthetizing mice with ketamine/xylazine. The primers used for genotyping (Integrated DNA Technologies, Coralville, IA) are included in **Supplemental table 1**.

Tamoxifen (Tam) treatment

At ~3 months of age, mice received a daily intraperitoneal (ip) injection of tamoxifen (Tam) solubilized in 100% sunflower seed oil by sonication (100 mg/kg body weight, 20 mg/ml stock solution, #T5648; Millipore Sigma, St. Louis, MO) for five consecutive days[12,14].

Lipopolysaccharide (LPS) treatment, protein sample preparation, and suspension array

At 3-4 weeks post-Tam treatment, Cx3cr1-cre/ERT2^{+}; NuTRAP^{+} mice were systemically administered 5 mg/kg LPS[31] (#L2262, 1 mg/ml stock solution; Millipore Sigma) or vehicle (PBS) by ip injection. Blood was collected from the facial vein of mice at 4h and 24h post-LPS treatment, using a 5-mm sterile Goldenrod animal lancet (MEDIpoint, Mineaola, NY), mixed with 5µl 0.5M EDTA to prevent coagulation[39], and centrifuged at 1,000 x g for 10 min for plasma collection. At 24h post LPS treatment, mice were euthanized and a sagittal slice circumscribing the medial line of their brains was harvested and homogenized in RIPA buffer supplemented with 1X Halt^{TM} protease inhibitor cocktail (#78437; ThermoFisher Scientific, Grand Island, NY) by sonication. The supernatants from tissue homogenates were assayed for protein content using a BCA protein

method (#23225; ThermoFisher Scientific) and along with diluted plasma samples, used for protein analyses. Suspension array analyte concentrations were determined using a Bio-Rad Bio-Plex System Luminex 100 and Bio-Plex manager 5.0 (Bio-Rad Laboratories, Hercules, CA)[40]. Milliplex Map luminex-based assays were used to quantify the mouse inflammatory cytokines IL-6, TNFα, and INFɣ (#MCYTOMAG-70K; EMD Millipore, Billerica, MA). The concentration of each analyte detected in plasma was expressed as log transformed (pg analyte/ml) and that detected in tissue homogenate as pg analyte/mg protein.

Flow cytometry

Halves of mouse brains were rinsed in D-PBS, sliced into 8-12 sagittal sections and placed into gentleMacs C-tubes, and processed for generation of single- cell suspensions using the Adult brain dissociation kit and gentleMacs™ Octodissociator system (#130-107-677 and #130-095-937, respectively, Milteny Biotech, San Diego, CA). The single-cell suspensions were then immunostained for flow cytometric analysis of $EGFP^+$ cell populations in the brain. The gating strategy of single cells was set to $EGFP^+/ACSA2^+$ for astrocytes **(Supplemental Figure 14)** and $EGFP^+/CD11b^+$ for microglia **(Supplemental Figure 15)**. A 488 nm (blue) laser with 530/30 and 580/30 filter combinations was used to gate on $EGFP^+$ cells within single cells (singlets) without auto-fluorescence interference. Subsequent gating based on CD11b or ACSA-2 expression was done with 640 nm laser and 676/629 filter, or with 488 nm laser and 740 LP filter combinations, respectively. The antibodies used were anti-mouse CD11b: APC (#17-0112, clone M1/70) (eBioscience, San Diego, CA), and ACSA-2: PE-Vio770 (#130-116-246, Milteny Biotec)[15]. Isotype controls for each antibody and unstained cells were used for proper post-color compensation **(Supplemental Figures 14-15)**. Samples were analyzed using a Stratedigm S1400Exi flow cytometer platform (Stratedigm, San Jose, CA) and CellCapTure v5.0 RC12 and v4.1 RC10 software (Stratedigm) at the Laboratory for Molecular Biology and Cytometry Research core facility at OUHSC.

Immunochemistry and imaging

For immunohistochemistry (IHC), mouse brains were harvested and hemisected. Samples were fixed for a duration of 4h in 4% paraformaldehyde, embedded in 2% agarose, and vibratome-sectioned (Vibratome 3000 Sectioning System, The Vibratome Company, St. Louis, MO), as previously described[41]. Two-hundred µm-thick sections were permeated for 2h in PBS containing 3% BSA and 0.2% Triton, and processed for fluorescence immunostaining. The primary antibodies included rabbit anti-mCherry (#ab167453, 1:500, Abcam, Cambridge, MA), chicken

anti-GFAP (#ab4674, 1:1,000, Abcam), rabbit anti-NeuN (#ab177487, 1:200, Abcam), and rat anti-CD11b (#C227, 1:200, Leinco Technologies, St. Louis, MO). For confocal imaging of nuclei suspensions, unfixed, freshly isolated nuclei were mixed with DAPI solution. Sequential imaging of brain samples and freshly isolated nuclei was performed on an Olympus FluoView confocal laser-scanning microscope (FV1200; Olympus; Center Valley, PA) at the Dean McGee Eye Institute imaging core facility at OUHSC. Microscope and FLUOVIEW FV1000 Ver. 1.2.6.0 software (Olympus) settings were identical/similar for samples within experiments at same magnification. The experimental format files were .oif (4-channel capture) or .oib (2 or 3-channel capture). For brain samples, the final Z-stack generated was achieved at 1.14-1.26 µm step size with a total of 12-16 optical slices at 20X magnification (1X, 1.5X or 2X zoom) and/or 0.55-0.62 µm step size with a total of 23-26 optical slices at 40 X magnifications (1.5X zoom). For nuclei samples, the Z-stack was achieved at 1.16 µm step size with 6-8 optical slices at 20X magnification (2X zoom). Instrument settings for capture of raw images, as well as downstream processing (Adobe Photoshop CS5.1) of each raw image used for figure assembly are disclosed under the **Supplemental table 7**: equipment and settings.

Isolation of Nuclei from Tagged specific nuclei (INTACT) and gDNA extraction

The purification of viable, cell-specific nuclei from brain tissue from Tam-induced Aldh1l1-cre/ERT2^{+}; NuTRAP^{+} and Cx3cr1-cre/ERT2^{+}; NuTRAP^{+} mice was achieved by combining two previously published protocols, with modifications[10,42]. For each mouse, a hemisected half-brain was rinsed in ice-cold 1X PBS, minced into small pieces and homogenized in 4 ml ice-cold nuclei EZ lysis buffer (#NUC-101, Millipore Sigma) supplemented with 1X Halt^{TM} protease inhibitor cocktail (ThermoFisher Scientific) using a glass dounce tissue grinder set (#D9063; Millipore Sigma: 20 times with pestle A and 20 times with pestle B)[42]. Undissociated tissue, largely composed of blood vessels, was removed by centrifugation at 200 x g for 1.5 min at 4°C[43], and the supernatant containing the nuclear material filtered through a 30 µm strainer and centrifuged at 500 x g for 5 min at 4°C. The resulting nuclear pellet was resuspended in nuclei lysis EZ buffer, incubated on ice for 5 min, washed by centrifugation, and resuspended in 300 µl nuclei EZ storage buffer by gentle trituration with a micropipette. From the total resuspended pellet volume, 10% was reserved as input nuclei fraction and the rest was diluted with 1.6 ml nuclei purification buffer (NPB: 20 mM HEPES, 40 mM NaCl, 90 mM KCl, 2 mM EDTA, 0.5 mM EGTA, 1X Halt^{TM} protease inhibitor cocktail), and subjected to the INTACT protocol[10]. Briefly, 30 µl of resuspended M-280 Streptavidin Dynabeads (#11205, ThermoFisher Scientific) were added into a fresh 2 ml microcentrifuge tube and washed with 1ml of NPB using a DynaMag-2 magnet (#12321;

ThermoFisher Scientific) for a total of three washes (1 min incubation/each). The washed beads were reconstituted to their initial volume (30 µl) with NPB and gently mixed with the nuclear suspension. The mixture of nuclei and magnetic beads was incubated at 4°C for 40 min under gentle rotation settings to allow the affinity binding of streptavidin beads to the cell-specific, biotinylated nuclei. After incubation, the streptavidin-bound nuclei were magnetically separated with the DynaMag-2 magnet for a period of 3 min and the unbound nuclei collected in a fresh 2 ml microcentrifuge tube, centrifuged at 4°C (1,000 x g, 3 min), resuspended in 100 µl of NPB and reserved as the negative nuclei fraction. The nuclei bound to the beads were washed in the magnet for three washes (1 min/each), resuspended in 30 µl of NPB, and reserved as the positive nuclei fraction. From each nuclear fraction (input, negative, and positive), a 3 µl aliquot was mixed with equal volume of DAPI counterstain and used for confocal microscopy visualization and calculation of purity percentage (3-5 fields of view per sample). The AllPrep DNA/RNA kit Micro (#80284, Qiagen, Germantown, MD) was used to extract gDNA from each sample[10]. gDNA was quantified with a Nanodrop 2000c spectrophotometer (Thermofisher Scientific) and its quality assessed by genomic DNA D1000 (#5067-5582) with a 2200 Tapestation analyzer (Agilent Technologies, Santa Clara, CA).

Bisulfite amplicon sequencing (BSAS)

INTACT-isolated gDNA samples (input, negative fraction, and positive fraction) and mouse methylation controls (#80-8063-MGHM-5 and #80-8064-MGUM-5; EpigenDX, Hopkinton, MA) were diluted in nuclease free elution buffer (Qiagen) to a 10 ng/µl concentration (200 ng gDNA in 20 µl final volume). DNA was bisulfite converted for methylation analysis with the EZ DNA Methylation-Lightning™ Kit (#D5030T; Zymo Research, Irvine, CA), according to the manufacturer's guidelines. For methylation quantitation of gene promoters, primer sets (Integrated DNA Technologies; **Supplemental Table 2**) were designed based on the appropriate National Center for Biotechnology Information (NCBI) reference genome using the Methyl Primer Express v1.0 software (Thermofisher Scientific) to amplify 250-350 bp regions of interest upstream or downstream the transcription start site (TSS) from bisulfite converted DNA, as previously described[44]. Bisulfite specific PCR optimization protocols were run to amplify and visualize amplicons by HSD1000 Tapestation. PCR amplicons were cleaned with Agencourt AmpureXP beads (#A63882; Beckman Coulter Life Sciences, Indianapolis, IN) using a two-sided size selection with 0.7X bead ratio followed by 0.15X bead ratio. Following clean-up, the amplicons were quantified using Qubit™ dsDNA HS assay kit (#Q32851; Thermofisher Scientific) and 5 ng of each amplicon was pooled per sample. One ng of the pooled amplicons was used for

library construction with the Nextera XT DNA library preparation kit (#FC-131-1096; Illumina, San Diego, CA), according to the manufacturer's guidelines. Libraries were quantified with Qubit™ dsDNA HS assay kit and TapeStation HD1000, normalized to 1 nM or 4 nM, and pooled for sequencing. Pooled libraries were then sequenced on iSeq or MiSeq (Illumina) at loading concentrations 35 pM or 8 pM, respectively. Fastq files were aligned to amplicon sequences in CLC Genomics Workbench 11.0 (Qiagen) using the "Map Bisulfite Reads to Reference" feature. Site-specific CpG (CG) and CH methylation percentages were extracted for downstream analysis.

Library construction and oxidative bisulfite sequencing (OxBS-seq)

Protocols were carried out as previously described[14]. For each input, negative, and positive INTACT-isolated sample 400 ng of gDNA was brought up to 50 µl volume with 1X low-EDTA TE buffer and sheared with a Covaris E220 sonicator (Covaris, Inc., Woburn, MA) to an average 200 base pair size using the following settings: intensity of 5, duty cycle of 10%, 200 cycles per burst, 2 cycles of 60 seconds, at 7 °C. The size of sheared products was confirmed by capillary electrophoresis (DNA D1000, Agilent). gDNA fragments were cleaned by an Agencourt bead-based purification protocol, after which gDNA was quantified (Qubit™ dsDNA, Thermofisher Scientific). Two aliquots of 200 ng gDNA fragments were prepared in a 12 µl volume to which 1µl of spike-in control DNA (0.08 ng/ul) with known levels of specific mC, hmC, and fC at individual sites was added. End repair, ligation of methylated adaptors (#L2V11DR-BC 1-96 adaptor plate, NuGEN, Tecan Genomics, Inc., Redwood City, CA) and final repair were performed according to manufacturer's instructions (Ovation Ultralow Methyl-Seq Library System, NuGEN). Of the two DNA aliquots per sample, one was oxidized and then bisulfite- converted and the other only bisulfite-converted with the True Methyl oxBS module (NuGEN) with desulfonation and purification. 22 µl of libraries were eluted from the magnetic beads. qPCR was used to determine the number (N) of PCR cycles required for library amplification. Bisulfite-converted samples were amplified for 7 cycles while oxidative bisulfite- converted samples were amplified for 11 cycles [95° C- 2 min, N (95°C-15 s, 60°C-1 min, 72° C-30s)]. Amplified libraries were purified with Agencourt beads and eluted in low-EDTA TE buffer. TapeStation HD1000 was used to validate and quantify libraries. Amplified libraries were normalized to a concentration of 4 nM and pooled, denatured, and diluted to 12 pM for sequencing on the NovaSeq 6000 (Illumina) according to manufacturer's guidelines with the exception of a custom sequencing primer (MetSeq Primer) that was spiked in with the Illumina Read 1 primer to a final concentration of 0.5 µM.

OxBS-seq data analysis

Global levels of mCG, hmCG, and mCH were analyzed as previously described.[14] Prior to alignment, paired-end reads were adaptor-trimmed and filtered using Trimmomatic[45] 0.35. End-trimming removed leading and trailing bases with Q-score<25, cropped 4 bases from the start of the read, dropped reads less than 25 bases long, and dropped reads with average Q-score<25 Alignment of trimmed bisulfite converted sequences was carried out using Bismark[46] 0.16.3 with Bowtie 2[47] against the mouse reference genome (GRCm38/mm10). Bams were de-duplicated using Bismark. Methylation call percentages for each CpG and non-CpG (CH) site within the genome were calculated by dividing the methylated counts over the total counts for that site in the oxidative bisulfite - converted libraries (OXBS). Genome-wide CpG and CH methylation levels were calculated separately. Hydroxymethylation levels in CpG (hmCG) and CH (hmCH) contexts were calculated by subtracting call levels from the oxidative bisulfite-converted (OXBS) libraries from the bisulfite-converted (BS) libraries. BAM files generated by MethylSeq (Basespace, Illumina) were run through MethylKit in R[48] to generate context-specific (CpG/CH) coverage text files. Bisulfite conversion efficiency for C, mC, and hmC was estimated using CEGX spike-in control sequences. Untrimmed fastq files were run through CEGX QC v0.2, which output a fastqc_data.txt file containing the conversion mean for C, mC, and hmC. Analysis of methylation levels in the proximity of the promoter region was performed on a list of selected genes as follows. The R package Enriched Heatmap[49] was used to intersect methylation call files with genomic coordinates of gene lists. Flanking regions of 4000 nucleotides were constructed upstream of the transcription start site (TSS) and downstream of the transcription end site (TES) and then split into 20 bins of 200 nucleotides each. The gene body was split into 27 equal bins, depending on the gene length. The average of each bin for all genes in the list was then plotted versus the bin number to give a visualization of the overall pattern of mCG within and around the genes contained in the gene lists. Average mCG and hmCG levels were calculated for the upstream region (-4kb to TSS), gene body (TSS to TES), and downstream region (TES to +4kb) for each gene list and biological replicate, and subjected to 2-way ANOVA statistical analysis with Sidak's multiple comparisons correction (GEO repository under accession code GSE140271).

Repeat element mCG, mCH, and hmCG was also examined. Repeat masker bed files were extracted from the UCSC Genome Browser Table Browser[50]. The context-specific CpG/CH MethylKit text files were intersected with the repeat masker bed files using 'bedtools', and percent methylation was calculated by dividing the average percent methylation at all common sites by

the total number of sites. This was done for long interspersed nuclear elements (LINE), short interspersed nuclear elements (SINE), long terminal repeats (LTR), and simple repeats.

Translating Ribosome Affinity Purification (TRAP) and RNA extraction

The purification of cell-specific RNA from brain tissue from Tam-induced Aldh1l1-cre/ERT2^{+}; NuTRAP^{+} and Cx3cr1-cre/ERT2^{+}; NuTRAP^{+} mice was achieved by following an established protocol, with slight modifications[11,51,52]. For each mouse, a hemisected half-brain was minced into small pieces and homogenized in 2 ml ice-cold homogenization buffer (50 mM Tris, pH 7.4; 12 mM MgCl2; 100 mM KCl; 1% NP-40; 1 mg/ml sodium heparin; 1 mM DTT) supplemented with 100 ug/mL cycloheximide (#C4859-1ML, Millipore Sigma), 200 units/ml RNaseOUT™ Recombinant Ribonuclease Inhibitor (#10777019; Thermofisher), and 1X cOmplete™, EDTA-free Protease Inhibitor Cocktail (#11836170001; Millipore Sigma) with a glass dounce tissue grinder set (#D8938; 10 times with pestle A and 10 times with pestle B). Homogenate was transferred to a 2 mL round-bottom tube and centrifuged at 12,000 x g for 10 minutes at 4°C. After centrifugation, 100 uL of the supernatant was saved as input. The remaining supernatant was transferred to a 2 mL round-bottom tube and incubated with 5 µg/µl of anti-GFP antibody (ab290; Abcam) at 4°C with end-over-end rotation for one hour. Dynabeads™ Protein G for Immunoprecipitation (#10003D; Thermofisher) were washed three times in 1 ml ice-cold low-salt wash buffer (50mM Tris, pH 7.5; 12mM MgCl2; 100mM KCl; 1% NP-40; 100µg/ml cycloheximide; 1mM DTT). After removal of the last wash, the homogenate/antibody mixture was transferred to the 2 ml round-bottom tube containing the washed Protein-G Dynabeads and incubated at 4°C with end-over-end rotation for an additional two hours. Magnetic beads were collected using a DynaMag-2 magnet and the unbound- ribosomes and associated RNA saved as the “negative” fraction. Beads were then washed three times with 1 ml of high-salt wash buffer (50mM Tris, pH 7.5; 12mM MgCl2; 300mM KCl; 1% NP-40; 100µg/ml cycloheximide; 2mM DTT). Following the last wash, 350 uL of Buffer RLT (Qiagen) supplemented with 3.5 µl 2-β mercaptoethanol was added directly to the beads and incubated with mixing on a ThermoMixer (Eppendorf) for 10 minutes at room temperature. The beads were magnetically separated and the supernatant containing the target bead-bound ribosomes and associated RNA was transferred to a new tube. 350 µl of 100% ethanol was added to the tube (“positive” fraction) and then loaded onto an RNeasy MinElute column. RNA was isolated using RNeasy Mini Kit (#74104, Qiagen), according to manufacturer’s instructions. RNA was quantified with a Nanodrop 2000c spectrophotometer (Thermofisher Scientific) and its quality assessed by HSRNA screentape with a 2200 Tapestation analyzer (Agilent Technologies).

638 **Library construction and RNA sequencing (RNA-seq)**

639 The NEBNext Ultra II Directional Library Prep Kit for Illumina (#NEBE7760L; New England Biolabs
640 Inc., Ipswich, MA) was used on 25 ng of total RNA for the preparation of strand-specific
641 sequencing libraries from each TRAP-isolated RNA sample (input, negative fraction, and positive
642 fraction) and from conventionally isolated RNA samples from brain (tissue), according to
643 manufacturer's instructions. Briefly, polyA containing mRNA was purified using oligo-dT attached
644 magnetic beads. mRNA was chemically fragmented and cDNA synthesized. For strand-
645 specificity, the incorporation of dUTP instead of dTTP in the second strand cDNA synthesis does
646 not allow amplification past this dUTP with the polymerase. Following cDNA synthesis, each
647 product underwent end repair process, the addition of a single 'A' base, and finally ligation of
648 adapters. The cDNA products were further purified and enriched using PCR to make the final
649 library for sequencing. Library sizing was performed with HS RNA ScreenTape (#5067-5579;
650 Agilent Technologies) and libraries were quantified by qPCR (Kappa Biosystems, Inc.,
651 Wilmington, MA). The libraries for each sample were pooled at 4 nM concentration and
652 sequenced using an Illumina NovaSeq 6000 system (SP PE50bp) at the Oklahoma Medical
653 Research Foundation Genomics Facility.

654 **RNA-Seq Data Analysis**

655 Following sequencing, reads were trimmed, aligned, differential expression statistics and
656 correlation analyses were performed in Strand NGS software package (Agilent), as previously
657 described[14]. Reads were aligned against the Mm10 build of the mouse genome (2014.11.26).
658 Alignment and filtering criteria included: adapter trimming, fixed 2bp trim from 5' and 6bp from 3'
659 ends, a maximum number of one novel splice allowed per read, a minimum of 90% identity with
660 the reference sequence, a maximum of 5% gap, trimming of 3' end with Q<30. Alignment was
661 performed directionally with Read 1 aligned in reverse and Read 2 in forward orientation. Reads
662 were filtered based on the mapping status and only those reads that aligned normally (in the
663 appropriate direction) were retained. Normalization was performed with the DESeq algorithm[53].
664 Transcripts with an average read count value >20 in at least 100% of the samples in at least one
665 group were considered expressed at a level sufficient for quantitation per tissue and those
666 transcripts below this level were considered not detected/not expressed and excluded, as these
667 low levels of reads are close to background and are highly variable. For statistical analysis of
668 differential expression, a one-way ANOVA or two-way ANOVA with the factors of TRAP fraction
669 and treatment and a Benjamini-Hochberg Multiple Testing Correction followed by Student-
670 Newman Keuls post hoc test were used. For those transcripts meeting this statistical criterion, a

fold change >|1.25| cutoff was used to eliminate those genes which were statistically significant but unlikely to be biologically significant and orthogonally confirmable due to their very small magnitude of change. Visualizations of hierarchical clustering and principle components analysis were performed in Strand Next Generation Analysis Software (NGS) (Version 3.1, Bangalore, India). The entirety of the sequencing data is available for download in FASTQ format from NCBI Sequence Read Archive (GSE140895 and GSE140974). Cell type specific maker gene lists were generated from the re-analysis published by McKenzie et al.[18] of immunopurified[54] and high throughput single cell data from mice[55,56]. Published lists were filtered first by mean enrichment score of ≥3.5 and secondly to remove any genes that appeared on lists for multiple cell types. Comparisons of astrocyte gene enrichment in this study to previously published Aldh1l1-RiboTag[12] and Gfap-TRAP[19] were performed by downloading raw fastq files with GEO accession numbers GSE84540 and GSE99791, respectively, and processing the files through StrandNGS as above, with minor alterations as necessitated by the type of sequencing data. After alignment, astrocyte markers were classified by differential expression between the input and positive fractions of Aldh1l1-RiboTag, Aldh1l1-TRAP, and Aldh1l1-NuTRAP was assessed by T-test, BHMTC<0.05 and FC>5. The intersection of these gene lists was then used to construct a ribosomal-tagging astrocyte gene list. In a similar manner, microglial marker genes identified in this study (t-test, BHMTC p<0.05 and FC(pos/input)>5) were compared to Cx3cr1(Jung)-RiboTag[5] and Cx3cr1(Litt)-TRAP[3] by downloading raw fastq files with GEO accession numbers GSE114001 and GSE108356, respectively, and processing as above. Gene expressions of selected genes from previously published gene lists[12,19,20] were imported into the IPA software Ingenuity Pathway Analysis (IPA) 01.12 (Qiagen Bioinformatics) to assess pathway/biological function enrichment analysis.

Quantitative PCR (qPCR)

Confirmation of gene expression levels was performed with qPCR as previously described[14,57,58]. cDNA was synthesized with the ABI High-Capacity cDNA Reverse Transcription Kit (Applied Biosystems Inc., Foster City, CA) from 25ng of purified RNA. qPCR was performed with gene-specific primer probe fluorogenic exonuclease assays (TaqMan, Life Technologies, Waltham, MA, **Supplemental table 3**) and the QuantStudio™ 12K Flex Real-Time PCR System (Applied Biosystems). Relative gene expression (RQ) was calculated with Expression Suite v 1.0.3 software using the $2^{-\Delta\Delta}$Ct analysis method with GAPDH as an endogenous control.

Stable Isotope Labeling

Microglial proliferation was measured as incorporation of deuterium into purine deoxyribose as previously described[59]. Briefly, mice were given an intraperitoneal injection of 99.9% D_2O and subsequently provided drinking water enriched with 8% D_2O for 30 days. Following INTACT isolation, DNA was extracted from nuclei using QiAamp DNA mini kit (Qiagen, Valencia, CA) according to manufacturer protocol. Extracted DNA was hydrolyzed overnight at 37 °C with nuclease S1 and potato acid phosphatase. Hydrolysates were prepared for analysis of the pentafluorobenzyl-*N*,N-di(pentafluorobenzyl) derivative of deoxyribose by GC-MS. Enrichment of deuterium in DNA from bone marrow was similarly analyzed for each animal to determine precursor enrichment. Fraction of new DNA was calculated based on the product/precursor relationship.

Data availability

Sequencing data that support the findings of this study have been deposited in GEO repository with the GSE140271 (https://www.ncbi.nlm.nih.gov/geo/query/acc.cgi?acc=GSE140271) accession code for information on oxBS-seq data (used for Figure 7 and Supplemental Figures 8 and 9). The entirety of the RNA-sequencing data is available for download in FASTQ format from NCBI Sequence Read Archive (GSE140895 and GSE140974). Other data that support the findings of the study are available from the corresponding author (W.M.F.) upon reasonable request.

Statistics

Datasets with groups of $n < 10$ were analyzed using GraphPad Prism version 8.2.0 (435) (San Diego, CA) and represented as dot plots with underlying bar graph with mean ± s.e.m. (standard error of the mean) or box plots consisting of median (boxes spanning Q1–Q3 and whiskers to the maximum and minimum value). Further information on research design is available in the Nature Research Reporting Summary linked to this article and in **Supplementary Table 6**.

Author contributions

Ana J. Chucair-Elliott: co-first author, design of the work, execution of experiments, data acquisition, analysis, and interpretation, figure generation, manuscript writing and preparation

Sarah R. Ocanas: co-first author, design of the work, execution of experiments, data acquisition, analysis, and interpretation, figure generation, manuscript writing and preparation

David R. Stanford: data analysis

Victor A. Ansere: execution of experiments, data acquisition, and analysis

Kyla B. Buettner: execution of experiments, data acquisition, and analysis

Hunter Porter: data analysis

Nicole L. Eliason: execution of experiments, data acquisition, and analysis

Justin Reid: execution of experiments, data acquisition, and analysis

Amanda L. Sharpe: conceptual design of the study, data interpretation, manuscript writing

Michael B. Stout: conceptual design of the study, data interpretation, manuscript writing

Michael J. Beckstead: conceptual design of the study, data interpretation, manuscript writing

Benjamin F. Miller: conceptual design of the study, data interpretation, manuscript writing

Arlan Richardson: conceptual design of the study, data interpretation, manuscript writing

Willard M. Freeman: Corresponding author, conceptual design of the study, data analysis and interpretation, figure generation, manuscript writing, preparation, and submission.

Competing Interest statements

Ana J. Chucair-Elliott: None

Sarah R. Ocanas: None

David R. Stanford: None

Victor A. Ansere: None

Kyla B. Buettner: None

Hunter Porter: None

Nicole L. Eliason: None

Justin Reid: None

Amanda L. Sharpe: None

Michael B. Stout: None

Michael J. Beckstead: None

Benjamin F. Miller: None

Arlan Richardson: None

Willard M. Freeman: None

References

1. Lister, R., *et al.* Global epigenomic reconfiguration during mammalian brain development. *Science* **341**, 1237905 (2013).
2. Mo, A., *et al.* Epigenomic Signatures of Neuronal Diversity in the Mammalian Brain. *Neuron* **86**, 1369-1384 (2015).
3. Ayata, P., *et al.* Epigenetic regulation of brain region-specific microglia clearance activity. *Nat Neurosci* **21**, 1049-1060 (2018).
4. Luo, C., *et al.* Single-cell methylomes identify neuronal subtypes and regulatory elements in mammalian cortex. *Science* **357**, 600-604 (2017).
5. Haimon, Z., *et al.* Re-evaluating microglia expression profiles using RiboTag and cell isolation strategies. *Nat Immunol* **19**, 636-644 (2018).
6. van den Brink, S.C., *et al.* Single-cell sequencing reveals dissociation-induced gene expression in tissue subpopulations. *Nat Methods* **14**, 935-936 (2017).
7. Angermueller, C., *et al.* Parallel single-cell sequencing links transcriptional and epigenetic heterogeneity. *Nat Methods* **13**, 229-232 (2016).
8. Heiman, M., *et al.* A translational profiling approach for the molecular characterization of CNS cell types. *Cell* **135**, 738-748 (2008).
9. Sanz, E., *et al.* Cell-type-specific isolation of ribosome-associated mRNA from complex tissues. *Proc Natl Acad Sci U S A* **106**, 13939-13944 (2009).
10. Deal, R.B. & Henikoff, S. The INTACT method for cell type-specific gene expression and chromatin profiling in Arabidopsis thaliana. *Nat Protoc* **6**, 56-68 (2011).
11. Roh, H.C., *et al.* Simultaneous Transcriptional and Epigenomic Profiling from Specific Cell Types within Heterogeneous Tissues In Vivo. *Cell Rep* **18**, 1048-1061 (2017).
12. Srinivasan, R., *et al.* New Transgenic Mouse Lines for Selectively Targeting Astrocytes and Studying Calcium Signals in Astrocyte Processes In Situ and In Vivo. *Neuron* **92**, 1181-1195 (2016).
13. Yona, S., *et al.* Fate mapping reveals origins and dynamics of monocytes and tissue macrophages under homeostasis. *Immunity* **38**, 79-91 (2013).
14. Chucair-Elliott, A.J., *et al.* Tamoxifen induction of Cre recombinase does not cause long-lasting or sexually divergent responses in the CNS epigenome or transcriptome: implications for the design of aging studies. *Geroscience* (2019).
15. Kantzer, C.G., *et al.* Anti-ACSA-2 defines a novel monoclonal antibody for prospective isolation of living neonatal and adult astrocytes. *Glia* **65**, 990-1004 (2017).
16. Sun, W., *et al.* SOX9 Is an Astrocyte-Specific Nuclear Marker in the Adult Brain Outside the Neurogenic Regions. *J Neurosci* **37**, 4493-4507 (2017).
17. Verkhratsky, A. & Nedergaard, M. Physiology of Astroglia. *Physiol Rev* **98**, 239-389 (2018).
18. McKenzie, A.T., *et al.* Brain Cell Type Specific Gene Expression and Co-expression Network Architectures. *Sci Rep* **8**, 8868 (2018).
19. Boisvert, M.M., Erikson, G.A., Shokhirev, M.N. & Allen, N.J. The Aging Astrocyte Transcriptome from Multiple Regions of the Mouse Brain. *Cell Rep* **22**, 269-285 (2018).
20. Itoh, N., *et al.* Cell-specific and region-specific transcriptomics in the multiple sclerosis model: Focus on astrocytes. *Proc Natl Acad Sci U S A* **115**, E302-E309 (2018).
21. O'Koren, E.G., Mathew, R. & Saban, D.R. Fate mapping reveals that microglia and recruited monocyte-derived macrophages are definitively distinguishable by phenotype in the retina. *Sci Rep* **6**, 20636 (2016).
22. Aguzzi, A., Barres, B.A. & Bennett, M.L. Microglia: scapegoat, saboteur, or something else? *Science* **339**, 156-161 (2013).

23. Yeh, H. & Ikezu, T. Transcriptional and Epigenetic Regulation of Microglia in Health and Disease. *Trends Mol Med* **25**, 96-111 (2019).
24. Sabbagh, M.F.*, et al.* Transcriptional and epigenomic landscapes of CNS and non-CNS vascular endothelial cells. *Elife* **7**(2018).
25. Hadad, N.*, et al.* Absence of genomic hypomethylation or regulation of cytosine-modifying enzymes with aging in male and female mice. *Epigenetics Chromatin* **9**, 30 (2016).
26. Wen, L.*, et al.* Whole-genome analysis of 5-hydroxymethylcytosine and 5-methylcytosine at base resolution in the human brain. *Genome Biol* **15**, R49 (2014).
27. Masser, D.R.*, et al.* Analysis of DNA modifications in aging research. *Geroscience* **40**, 11-29 (2018).
28. de Koning, A.P., Gu, W., Castoe, T.A., Batzer, M.A. & Pollock, D.D. Repetitive elements may comprise over two-thirds of the human genome. *PLoS Genet* **7**, e1002384 (2011).
29. Papin, C.*, et al.* Combinatorial DNA methylation codes at repetitive elements. *Genome Res* **27**, 934-946 (2017).
30. Bennett, M.L.*, et al.* New tools for studying microglia in the mouse and human CNS. *Proc Natl Acad Sci U S A* **113**, E1738-1746 (2016).
31. Clarke, L.E.*, et al.* Normal aging induces A1-like astrocyte reactivity. *Proc Natl Acad Sci U S A* **115**, E1896-E1905 (2018).
32. Zamanian, J.L.*, et al.* Genomic analysis of reactive astrogliosis. *J Neurosci* **32**, 6391-6410 (2012).
33. Kielian, T. Toll-like receptors in central nervous system glial inflammation and homeostasis. *J Neurosci Res* **83**, 711-730 (2006).
34. Cheray, M. & Joseph, B. Epigenetics Control Microglia Plasticity. *Front Cell Neurosci* **12**, 243 (2018).
35. Busch, R., Neese, R.A., Awada, M., Hayes, G.M. & Hellerstein, M.K. Measurement of cell proliferation by heavy water labeling. *Nat Protoc* **2**, 3045-3057 (2007).
36. Reu, P.*, et al.* The Lifespan and Turnover of Microglia in the Human Brain. *Cell Rep* **20**, 779-784 (2017).
37. Guneykaya, D.*, et al.* Transcriptional and Translational Differences of Microglia from Male and Female Brains. *Cell Rep* **24**, 2773-2783 e2776 (2018).
38. Ogilvy, S.*, et al.* Promoter elements of vav drive transgene expression in vivo throughout the hematopoietic compartment. *Blood* **94**, 1855-1863 (1999).
39. Chucair-Elliott, A.J., Carr, M.M. & Carr, D.J.J. Long-term consequences of topical dexamethasone treatment during acute corneal HSV-1 infection on the immune system. *J Leukoc Biol* **101**, 1253-1261 (2017).
40. Chucair-Elliott, A.J., Gurung, H.R., Carr, M.M. & Carr, D.J.J. Colony Stimulating Factor-1 Receptor Expressing Cells Infiltrating the Cornea Control Corneal Nerve Degeneration in Response to HSV-1 Infection. *Invest Ophthalmol Vis Sci* **58**, 4670-4682 (2017).
41. Chucair-Elliott, A.J.*, et al.* Microglia-induced IL-6 protects against neuronal loss following HSV-1 infection of neural progenitor cells. *Glia* **62**, 1418-1434 (2014).
42. Habib, N.*, et al.* Massively parallel single-nucleus RNA-seq with DroNc-seq. *Nat Methods* **14**, 955-958 (2017).
43. Lopez-Sanchez, N. & Frade, J.M. Genetic evidence for p75NTR-dependent tetraploidy in cortical projection neurons from adult mice. *J Neurosci* **33**, 7488-7500 (2013).
44. Masser, D.R., Stanford, D.R. & Freeman, W.M. Targeted DNA methylation analysis by next-generation sequencing. *J Vis Exp* (2015).
45. Bolger, A.M., Lohse, M. & Usadel, B. Trimmomatic: a flexible trimmer for Illumina sequence data. *Bioinformatics* **30**, 2114-2120 (2014).

46. Krueger, F. & Andrews, S.R. Bismark: a flexible aligner and methylation caller for Bisulfite-Seq applications. *Bioinformatics* **27**, 1571-1572 (2011).
47. Langmead, B. & Salzberg, S.L. Fast gapped-read alignment with Bowtie 2. *Nat Methods* **9**, 357-359 (2012).
48. Akalin, A.*, et al.* methylKit: a comprehensive R package for the analysis of genome-wide DNA methylation profiles. *Genome Biol* **13**, R87 (2012).
49. Gu, Z., Eils, R., Schlesner, M. & Ishaque, N. EnrichedHeatmap: an R/Bioconductor package for comprehensive visualization of genomic signal associations. *BMC Genomics* **19**, 234 (2018).
50. Casper, J.*, et al.* The UCSC Genome Browser database: 2018 update. *Nucleic Acids Res* **46**, D762-D769 (2018).
51. Heiman, M., Kulicke, R., Fenster, R.J., Greengard, P. & Heintz, N. Cell type-specific mRNA purification by translating ribosome affinity purification (TRAP). *Nat Protoc* **9**, 1282-1291 (2014).
52. Kang, S.S.*, et al.* Microglial translational profiling reveals a convergent APOE pathway from aging, amyloid, and tau. *J Exp Med* **215**, 2235-2245 (2018).
53. Anders, S. & Huber, W. Differential expression analysis for sequence count data. *Genome Biol* **11**, R106 (2010).
54. Zhang, Y.*, et al.* An RNA-sequencing transcriptome and splicing database of glia, neurons, and vascular cells of the cerebral cortex. *J Neurosci* **34**, 11929-11947 (2014).
55. Tasic, B.*, et al.* Adult mouse cortical cell taxonomy revealed by single cell transcriptomics. *Nature Neuroscience* **19**, 335 (2016).
56. Zeisel, A.*, et al.* Cell types in the mouse cortex and hippocampus revealed by single-cell RNA-seq. *Science* **347**, 1138-1142 (2015).
57. Simpson, J.T.*, et al.* Detecting DNA cytosine methylation using nanopore sequencing. *Nature Methods* **14**, 407 (2017).
58. Masser, D.R.*, et al.* Hippocampal subregions exhibit both distinct and shared transcriptomic responses to aging and nonneurodegenerative cognitive decline. *J Gerontol A Biol Sci Med Sci* **69**, 1311-1324 (2014).
59. Miller, B.F., Drake, J.C., Naylor, B., Price, J.C. & Hamilton, K.L. The measurement of protein synthesis for assessing proteostasis in studies of slowed aging. *Ageing Res Rev* **18**, 106-111 (2014).

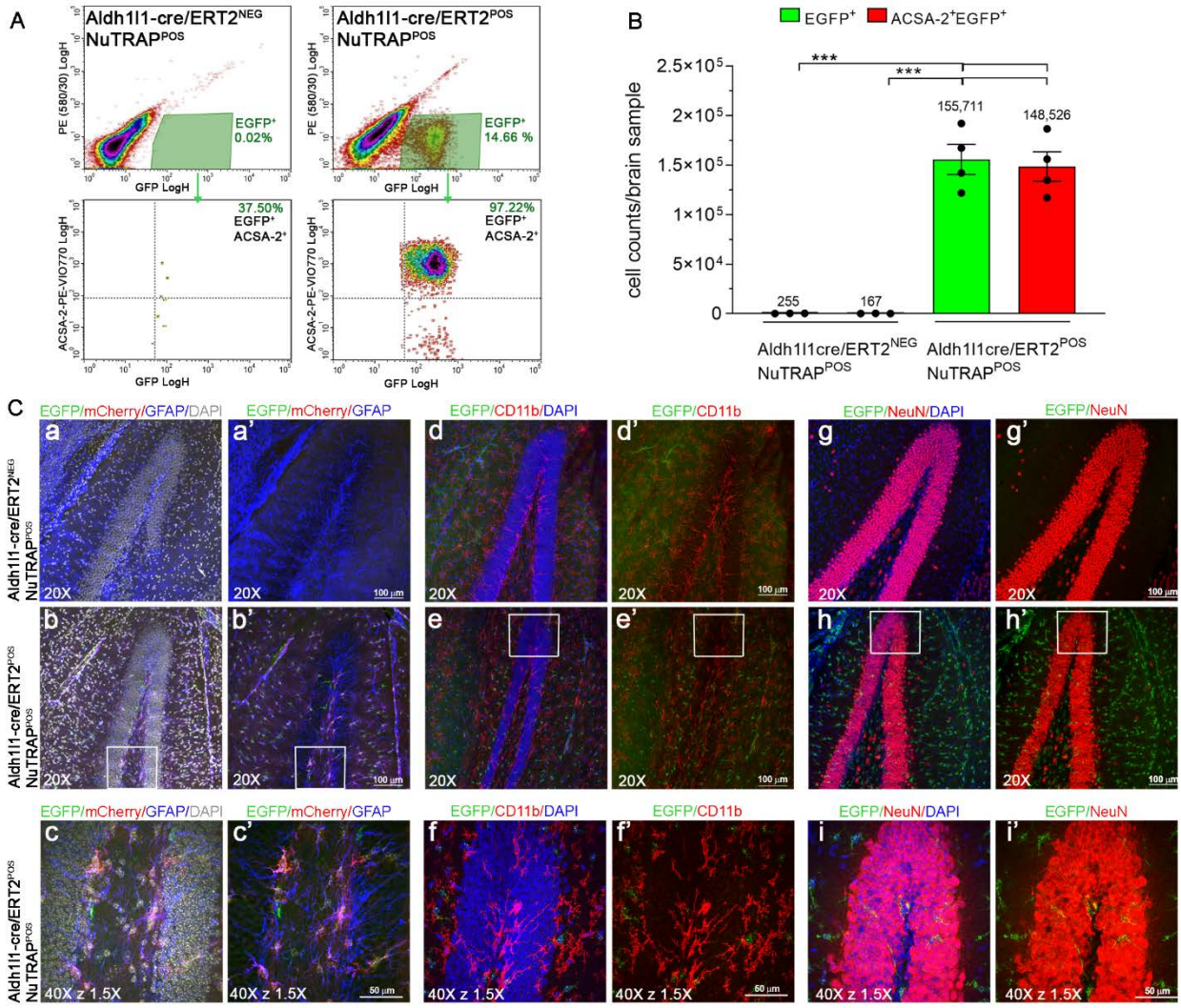

884 **Figure 1**. **Flow cytometry and immunohistochemical validation of the Aldh1l1-NuTRAP**
885 **transgene expression.** One week after Tam treatment, brains were harvested from Aldh1l1-
886 NuTRAP and cre negative NuTRAP$^+$ (control) mice for flow cytometry (FC) and
887 immunohistochemistry (IHC) purposes. A) Representative FC plots of immunostained single- cell
888 suspensions showed a distinct population of brain EGFP$^+$ cells, identified as Aldh1l1$^+$ cells
889 (astrocyte lineage), based on gating strategy for EGFP and ACSA-2 co-expression in Aldh1l1-
890 NuTRAP samples but not in the controls. B) Analysis of absolute cell counts from FC quantitation
891 expressed as mean cell count/brain sample ±SEM. C) Representative confocal fluorescent
892 microscopy images of sagittal brain sections show EGFP expression (green signal) in cells that
893 co-expressed mCherry (red signal) and GFAP (blue signal) in Aldh1l1-NuTRAP brains but did not
894 colocalize with other cell type marker expression. *** $p<0.001$ between depicted groups by one-
895 way ANOVA followed by the Tukey's multiple comparison test (n=4 for cre$^+$ group, n=3 for cre$^-$
896 group).

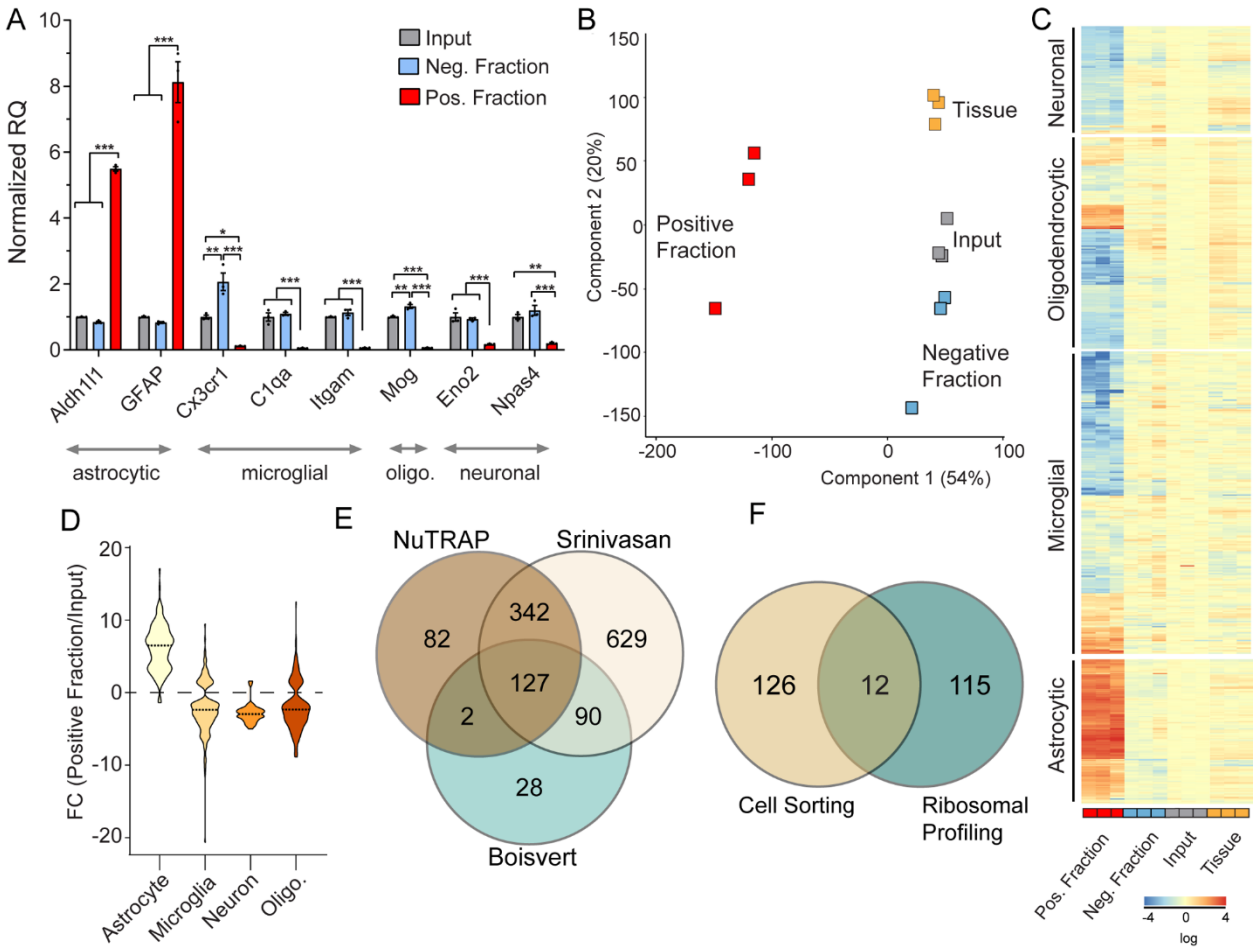

Figure 2. Transcriptomic validation of astrocytic enrichment in TRAP-RNA from Aldh1l1-NuTRAP mouse brain. A) TRAP-isolated RNA from input, TRAP-negative and TRAP-positive fractions were examined by qPCR for enrichment and depletion of selected cell-specific genes for astrocytes, microglia, neurons, and oligodendrocytes. Bar graphs represent mean relative gene expression ± SEM for each gene measured. *, **and *** $p<0.05$, $p<0.01$, $p<0.001$, respectively by one-way ANOVA with Benjamini-Hochberg multiple testing correction followed by Tukey's multiple comparison test across fractions (n=3/group). B) RNAseq analysis was performed on all fractions and total brain RNA (n=3/group). Principal component analysis of transcriptome profiles showed separation of positive fraction from input, negative, and tissue samples by the first component. C) Expression of cell-type marker gene lists, generated from cell sorting studies shows enrichment of astrocytic genes and depletion of other cell type genes in the positive fraction versus other fractions. D) Enrichment or depletion of marker genes is presented as the fold change (Positive fraction/Input). Astrocyte marker genes were enriched in the positive fraction while genes from other cell types were generally depleted in the positive faction relative to input. E) Astrocyte marker genes identified in prior Ribo-Tag analysis (FC>5 Positive fraction/Input) with the same cre line (Srinivasan)[12] and with a Gfap-Cre line (Boisevert)[19] were compared to the marker genes identified from the Aldh1l1-NuTRAP, demonstrating 127 ribosomal-tagging common astrocyte marker genes. F) The 127 astrocyte markers were then compared to astrocyte markers from cell sorting studies (McKenzie et al., 2018)[18] to identify 12 isolation method independent astrocyte markers.

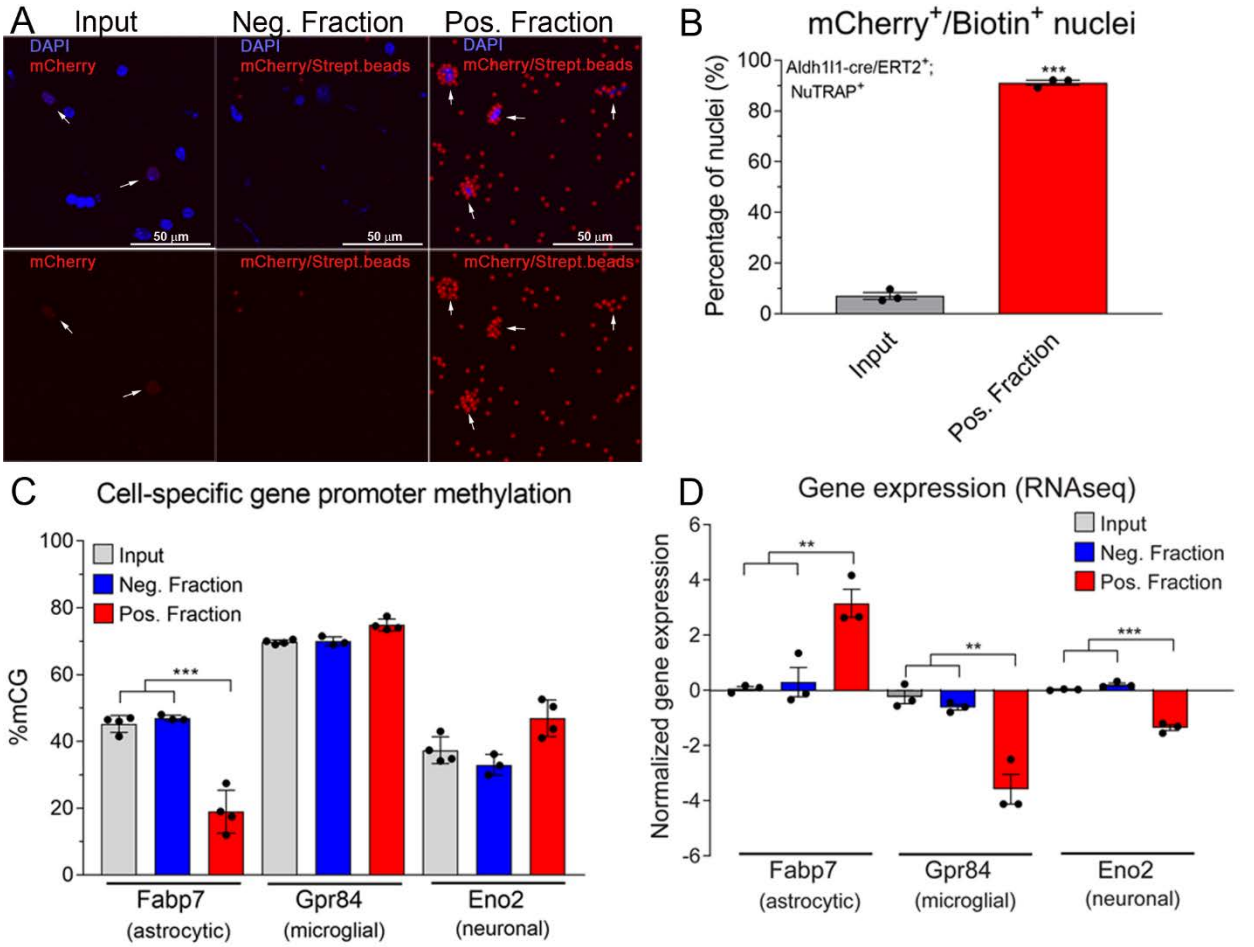

Figure 3. Validation of astrocytic nuclei and epigenome enrichment in the Aldh1l1-NuTRAP mouse brain by INTACT-BSAS. A) Representative confocal fluorescent microscopy images from input, negative, and positive INTACT nuclei fractions. B) Purity of astrocytic nuclei, expressed as average percentage ± SEM mCherry$^+$/ Biotin$^+$ nuclei in the positive fraction, compared to percentage ± SEM mCherry$^+$ nuclei in the input demonstrates a high degree of specificity to the INTACT isolation (n=3/group, ***p<0.001 by paired T test comparing positive fraction to input). C) INTACT-isolated genomic DNA from Aldh1l1-NuTRAP mice was bisulfite converted and DNA methylation in specific regions of interest (promoters for neuron, astrocytes and microglia marker genes) were analyzed by Bisulfite Amplicon Sequencing (BSAS) from input, negative, and positive fractions. Hypomethylation of the Fabp7 astrocyte marker gene in the positive fraction compared to input and negative fraction correlates with astrocytic enrichment (average % mCG ±SEM), as observed by RNA-seq (D), expressed as average normalized gene expression ±SEM. n=4/group in C and n=3/group in D. ***p<0.001, **p<0.01 by one-way ANOVA followed by the Tukey's multiple comparison test.

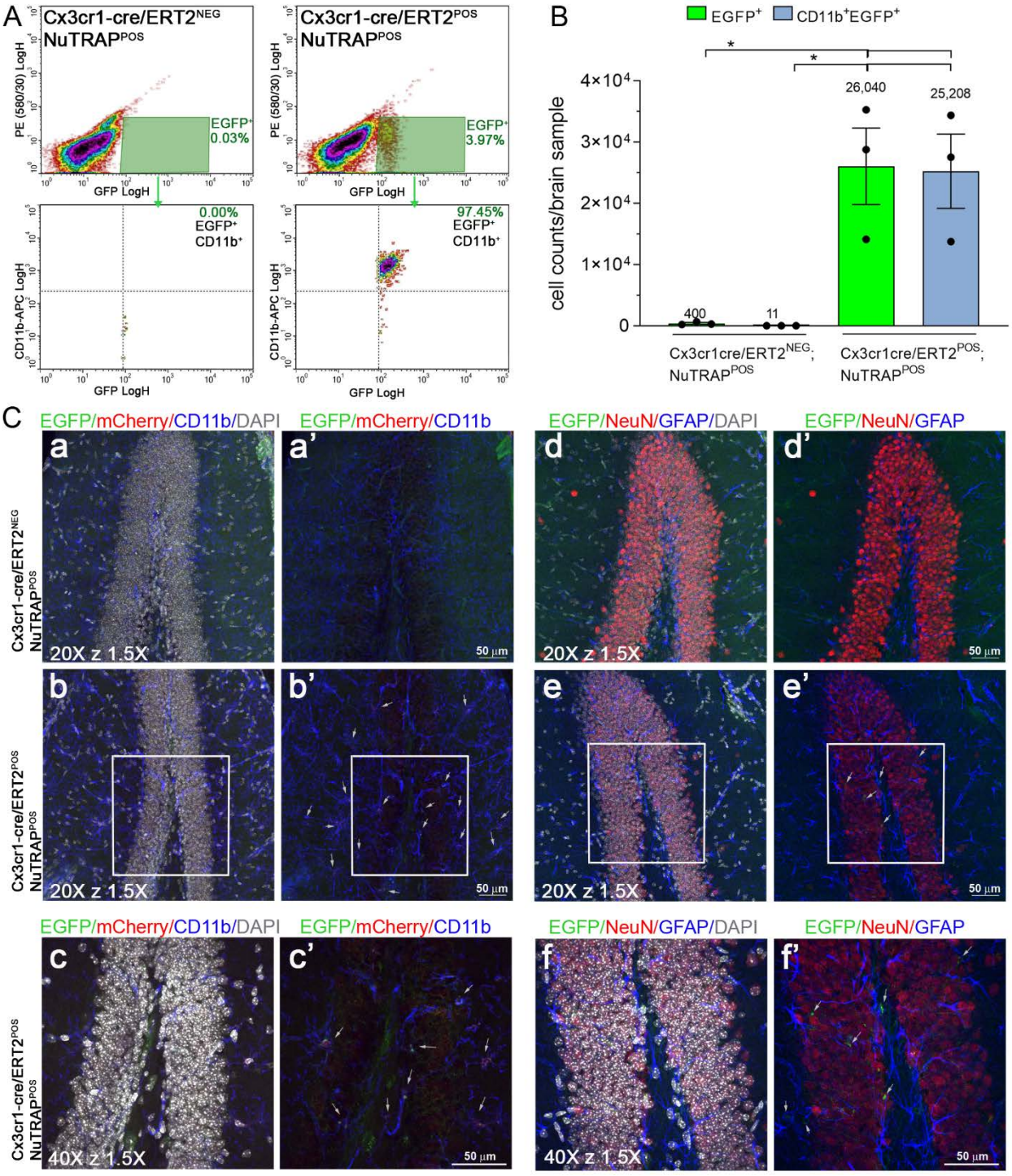

Figure 4. Flow cytometry and immunohistochemical validation of the Cx3cr1-NuTRAP mouse brain. After Tam treatment, brains from Cx3cr1-NuTRAP and cre negative NuTRAP^{+} (control) mice were harvested and single hemispheres assessed by flow cytometry (FC) and immunohistochemistry (IHC). A) Representative FC plots of immunostained single-cell suspensions showed a distinct population of brain EGFP^{+} cells, identified as CD11b^{+} cells (microglia lineage), based on gating strategy for EGFP and CD11b co-expression in Cx3cr1-NuTRAP samples upon cre-mediated recombination but not in the controls. B) Analysis of

absolute cell counts from FC quantitation expressed as mean cell count/brain sample ±SEM. C) Representative confocal fluorescent microscopy images of sagittal brain sections. EGFP expression (green signal) was found in cells that co-expressed mCherry (red signal) and CD11b (blue signal) in Cx3cr1-NuTRAP^{+} brains. * $p<0.05$ between depicted groups by one-way ANOVA followed by the Tukey's multiple comparison test (n=3/group).

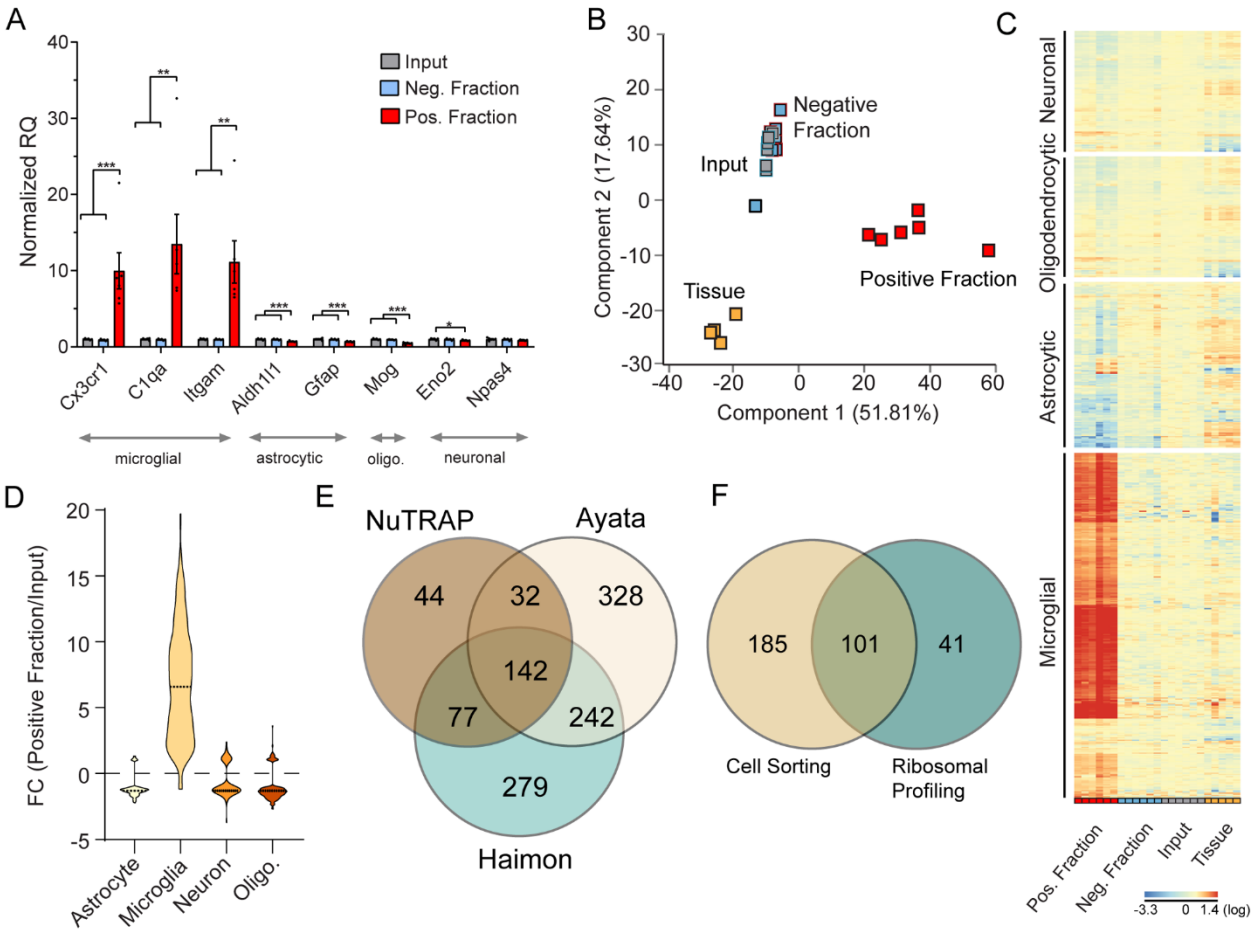

Figure 5. Validation of microglial TRAP-RNA enrichment in the Cx3cr1-NuTRAP mouse brain. A) TRAP-isolated RNA from input, negative, and positive fractions were examined by qPCR for enrichment/depletion of selected cell-specific genes for microglia, astrocytes, oligodendrocytes, and neurons. Bar graphs represent average relative gene expression ± SEM. *, **and *** p<0.05, p<0.01, p<0.001, respectively by one-way ANOVA with Benjamini-Hochberg procedure to correct for multiple comparisons of genes followed by Tukey's multiple comparison test of fractions (n=6/group). B) Principal component analysis of transcriptome profiles showed separation of positive fraction from input, negative and tissue samples by the first component. C) RNAseq heatmap graph of cell type marker genes from prior cell sorting studies shows enrichment of microglial marker genes and depletion of other cell type markers, as compared to whole tissue, input, and negative fractions. D) Marker gene lists for different cell types were generated from cell sorting studies as described in the text. Enrichment or depletion of genes from each of the lists is presented as the fold change (Positive fraction/Input). Microglial marker genes were enriched in the positive fraction while genes from other cell types were generally depleted in the positive fraction relative to input. E) Microglia marker genes with FC>5 (Positive fraction/Input) from the Cx3cr1-cre/ERT2^{+} model with RiboTag (Haimon)[5], Cx3cr1-cre/ERT2^{+} model with TRAP (Ayata)[3], and NuTRAP identifies 142 ribosomal-tagging common microglial marker genes. F) Comparison of the 142 common microglial markers with previously identified microglial markers from cell sorting studies (McKenzie)[18] identifies 101 isolation method-independent microglia marker genes.

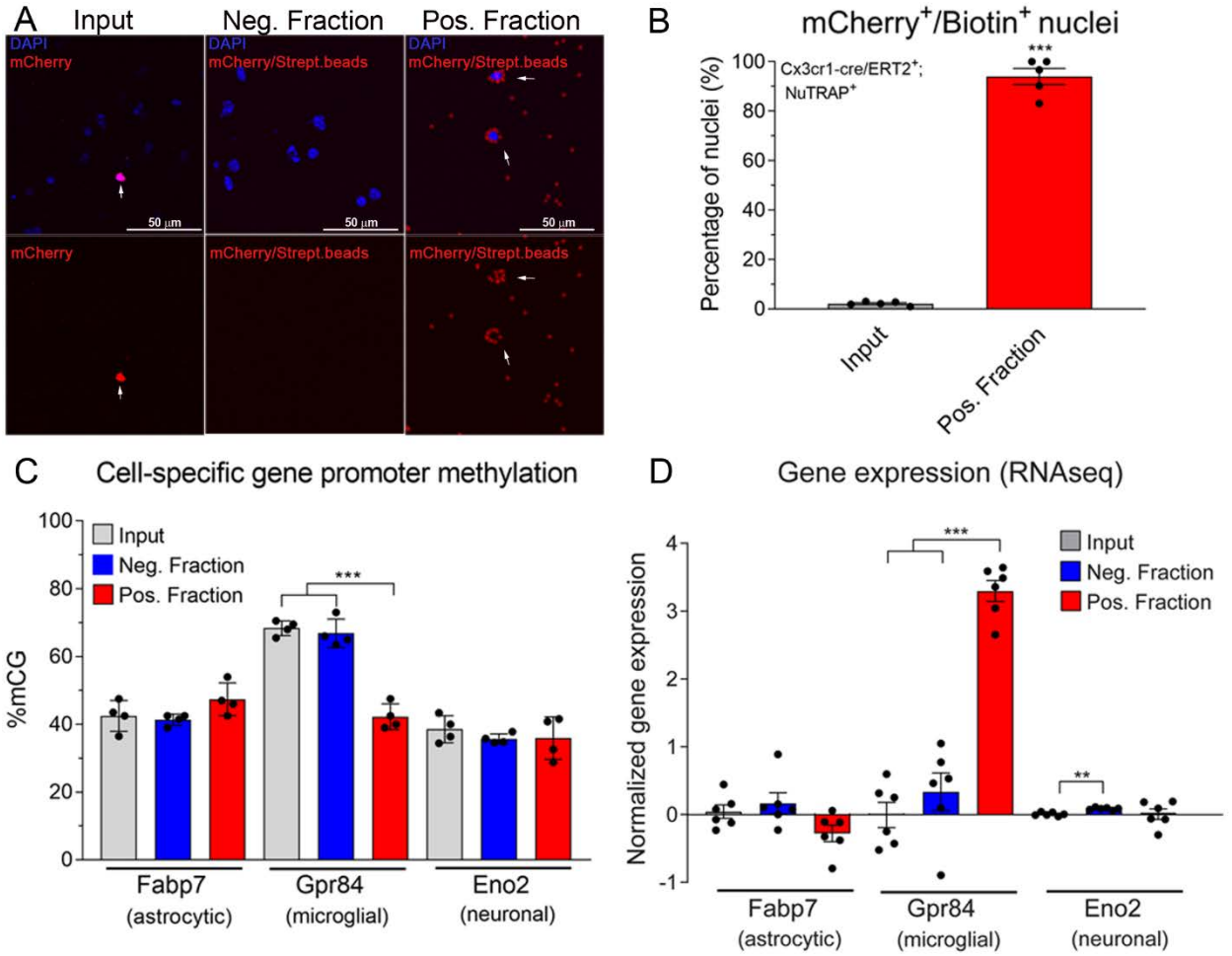

Figure 6. Validation of microglial epigenome enrichment in the Cx3cr1-NuTRAP mouse brain by INTACT-BSAS. A) Representative confocal fluorescent microscopy images from input, negative, and positive INTACT nuclei fractions. B) Purity of microglial nuclei expressed as average percentage ± SEM mCherry$^+$/ Biotin$^+$ nuclei in the positive fraction, and percentage ± SEM mCherry$^+$ nuclei in the input and average percentage ± SEM mCherry$^+$/Biotin$^+$ nuclei in the input demonstrates a high degree of specificity to the INTACT isolation (n=5/group, ***p<0.001 by paired T test comparing positive fraction to input). C) INTACT-isolated genomic DNA from Cx3cr1- NuTRAP mice was bisulfite converted and DNA methylation in specific regions of interest (promoters for neuron, astrocytes and microglia marker genes) were analyzed by Bisulfite Amplicon Sequencing (BSAS) from input, negative, and positive fractions. C) Hypomethylation of the Gpr84 microglial marker gene in the positive fraction compared to input and negative fraction correlates with microglial enrichment (average % mCG ±SEM), as observed by RNA-seq, expressed as average normalized gene expression ± SEM. D) n=4/group in C and n=6/group in D, **p<0.01, ***p<0.001, by one-way ANOVA followed by the Tukey's multiple comparison test.

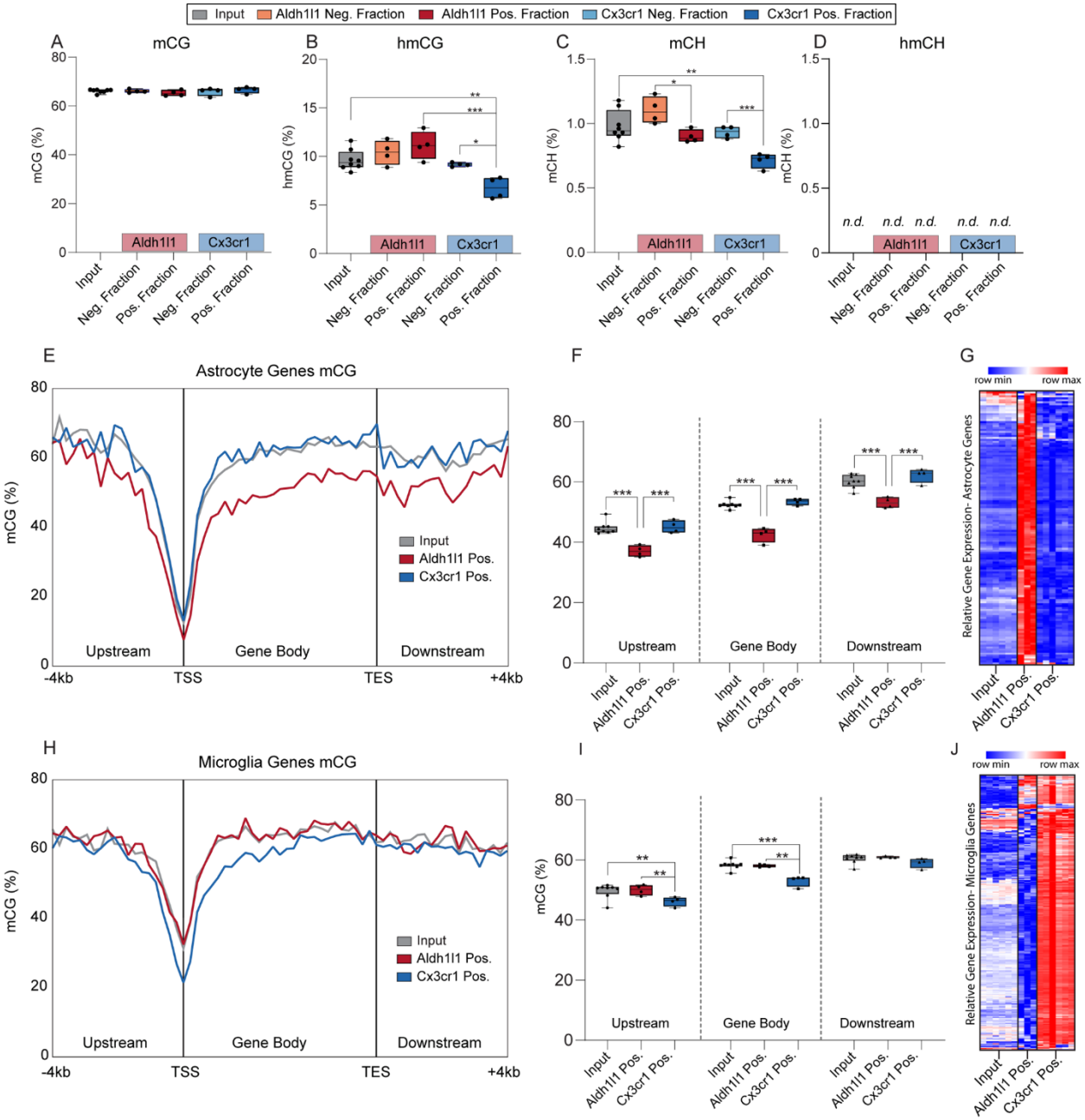

977 **Figure 7. DNA modification profiles of INTACT isolated DNA from Aldh1l1-NuTRAP and**
978 **Cx3cr1-NuTRAP mouse brains by WGoxBS.** INTACT-DNA samples from Aldh1l1-NuTRAP
979 and Cx3cr1-NuTRAP brains were used for epigenome analyses. A-D) Total genomic levels of
980 mCG, hmCG, mCH, and hmCH (n=8/input, n=4/positive fraction; One-way ANOVA with Tukey's
981 multiple comparisons test, *p<0.05, **p<0.01, ***p<0.001). E) mCG averaged over 200 nucleotide
982 bins upstream, in the gene body, and downstream of published astrocyte genes (McKenzie)[18] in
983 the positive fraction of Aldh1l1-NuTRAP, positive fraction of Cx3cr1-NuTRAP, and input samples
984 combined. F) Average percentage mCG in the positive fraction of Aldh1l1-NuTRAP, positive
985 fraction of Cx3cr1-NuTRAP , and input samples combined in genomic DNA upstream 4kb of the
986 TSS, in the gene body, and downstream 4kb of the TES of astrocytic genes G) Hypomethylation
987 of astrocytic gene promoters in the Aldh1l1-NuTRAP positive fraction correlates with higher

988 astrocytic gene expression in the Aldh1l1 positive fraction than input and Cx3cr1-NuTRAP
989 positive fraction. H) mCG averaged over 200 nucleotide bins upstream, in the gene body, and
990 downstream of published microglia genes[18] in the positive fraction of Aldh1l1-NuTRAP, positive
991 fraction of Cx3cr1-NuTRAP, and input. I) Average percentage mCG in the positive fraction of
992 Aldh1l1-NuTRAP, positive fraction of Cx3cr1-NuTRAP, and input DNA upstream 4kb of the TSS,
993 in the gene body, and downstream 4kb of the TES of microglia genes. J) Hypomethylation of
994 microglia gene promoters in the Cx3cr1 positive fraction correlates with higher microglia gene
995 expression. E-F-G-I) n=8/input, n=4/positive fraction; 2-way ANOVA with Sidak's multiple
996 comparison test, *$p<0.05$, **$p<0.01$, ***$p<0.001$.

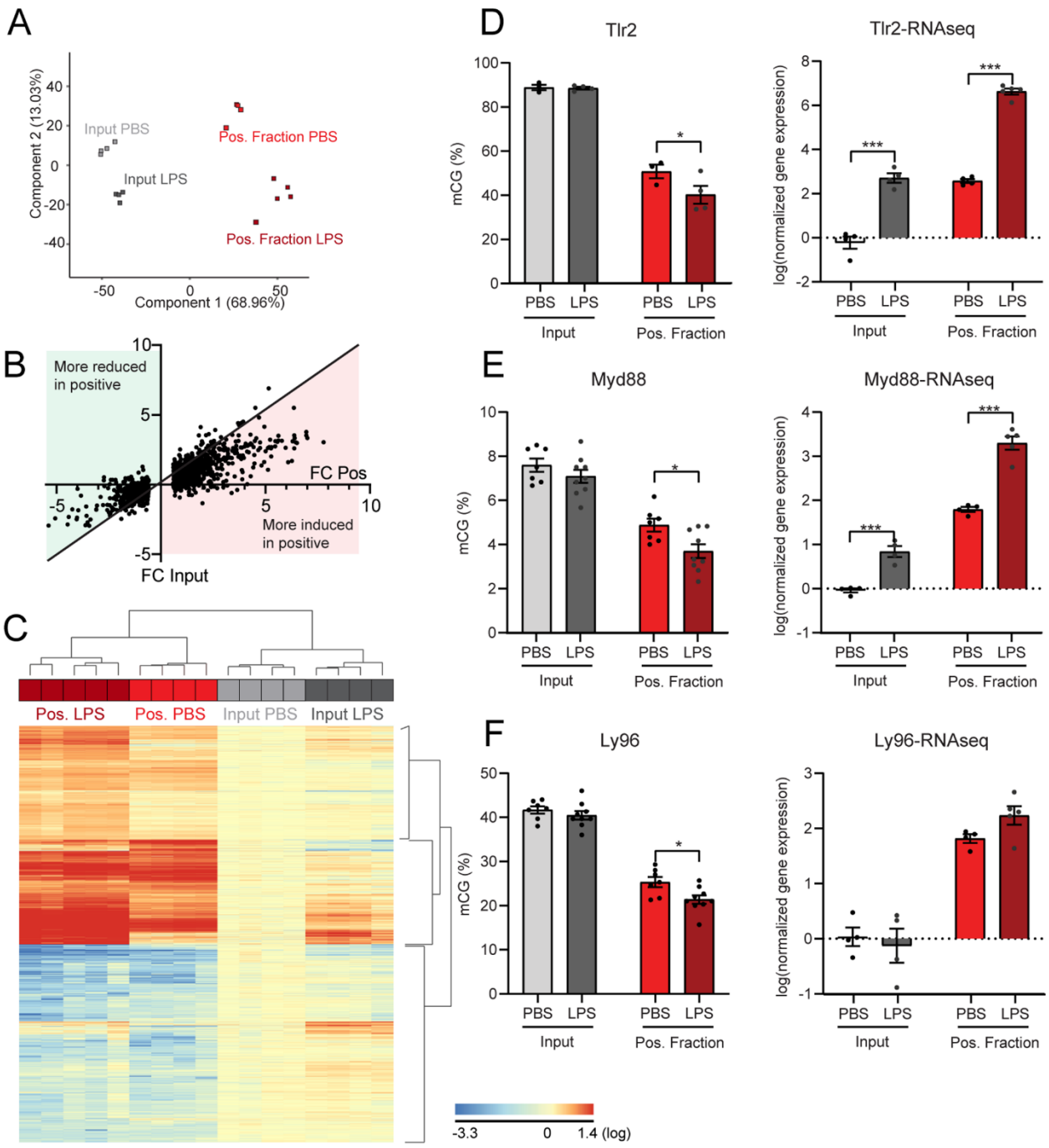

997 **Figure 8. RNAseq analysis of microglial transcriptome and targeted BSAS in specific gene**
998 **promoters 24 hours after LPS challenge in Cx3cr1-NuTRAP mouse brain.** Cx3cr1-NuTRAP
999 mice were treated with LPS or PBS as control for 24 hours. A) RNAseq was performed and
1000 principal component analysis of transcriptome profiles showed separation of positive fraction
1001 (PBS- and LPS-treated) from input (PBS- and LPS-treated) samples by the first component, as
1002 well as subclustering based on treatment within input and positive fraction samples by the second
1003 component. B) Fold change of genes differentially expressed after LPS in the positive fraction
1004 were compared to the fold change in the positive fraction. LPS induced larger changes when
1005 microglial RNA is isolated by TRAP. C) RNAseq heatmap graph of cell type marker genes from

prior cell sorting studies shows hierarchical clustering differentiating input from positive fractions and secondly comparing treatment within type of fraction. D-E) Tlr2 and Myd88 promoter methylation (mCG) decreases with LPS challenge in the positive fraction but not in the input, in correlation with increased Tlr2 and Myd88 gene expression in the positive fraction, as shown by RNAseq analysis. F) Although Ly96 promoter methylation decreases in the positive fraction with LPS challenge, there is no change in gene expression with LPS challenge in the input or positive fraction by RNA-seq. BSAS: n=4/group for Tlr2 and n=7/group for Ly96 and Myd88. RNA-seq: n=4/PBS groups, n=4/LPS input group, and n=5/LPS positive fraction group. *p<0.05, **p<0.01, ***p<0.001 by Multiple t-test with Holm-Sidak correction for multiple comparisons.